ÉCOLE POLYTECHNIQUE
FÉDÉRALE DE LAUSANNE

MATHICSE
Mathematics Institute of Computational Science and Engineering
School of Basic Sciences - Section of Mathematics

MATHICSE Technical Report
Nr. 16.2012
April 2012

Numerical comparison and calibration of geometrical multiscale models for the simulation of arterial flows

A.Cristiano I. Malossi, Jean Bonnemain

http://mathicse.epfl.ch

Phone: +41 21 69 37648

Address:
EPFL - SB - MATHICSE (Bâtiment MA)
Station 8 - CH-1015 - Lausanne - Switzerland

Fax: +41 21 69 32545

Biomech Model Mechanobiol manuscript No.
(will be inserted by the editor)

Numerical comparison and calibration of geometrical multiscale models for the simulation of arterial flows

A. Cristiano I. Malossi · Jean Bonnemain

Last version: April 5, 2012

Abstract Arterial tree hemodynamics can be simulated by means of several models of different level of complexity, depending on the outputs of interest and the desired degree of accuracy. In this work, several numerical comparisons of geometrical multiscale models are presented with the aim of evaluating the benefits of such complex dimensionally-heterogeneous models compared to other simplified simulations. More precisely, we present flow rate and pressure wave form comparisons between three-dimensional patient-specific geometries implicitly coupled with one-dimensional arterial tree networks and (i) a full one-dimensional arterial tree model and (ii) stand-alone three-dimensional fluid-structure interaction models with boundary data taken from precomputed full one-dimensional network simulations. On a slightly different context, we also focus on the set up and calibration of cardiovascular simulations. In particular, we perform sensitivity analyses of the main quantities of interest (flow rate, pressure, and solid wall displacement) in respect to the parameters accounting for the elastic and viscoelastic responses of the tissues surrounding the external wall of the arteries. Finally, we also compare the results of geometrical multiscale models in which the boundary solid rings of the three-dimensional geometries are fixed, in respect to those where the boundary interfaces are scaled to enforce the continuity of the vessels size with the surrounding one-dimensional arteries.

A. Cristiano I. Malossi · Jean Bonnemain
CMCS, Chair of Modelling and Scientific Computing,
MATHICSE, Mathematics Institute of Computational Science and Engineering, EPFL, École Polytechnique Fédérale de Lausanne,
Station 8, CH-1015, Lausanne, Switzerland,
E-mail: cristiano.malossi@epfl.ch

Jean Bonnemain
CHUV, Centre Hospitalier Universitaire Vaudois, Rue du Bugnon 21,
CH-1011, Lausanne, Switzerland

Keywords geometrical multiscale modeling · blood flow models · fluid-structure interaction · wave propagation · patient-specific geometries · aorta and iliac arteries

Mathematics Subject Classification (2000) 65M60 · 74F10 · 76D05 · 92C35

1 Introduction

Numerical simulations based on complex mathematical approaches have become an effective tool to model arterial flow dynamics. Research in this field is essential in order to understand, predict, and treat common and potentially fatal cardiovascular pathologies, such as aneurysms formation, atherosclerosis, and congenital defects, as well as the results of surgical interventions or medical treatments.

Being the time constraint important in a medical environment, a compromise between model complexity and computational cost is mandatory. In this sense, geometrical multiscale approaches provide an efficient and reliable way to select the desired level of complexity in each component of the cardiovascular system (see, e.g., Formaggia et al (1999), Vignon-Clementel et al (2006), Blanco et al (2007), Papadakis (2009), and Malossi et al (2012)). The main ingredients of a geometrical multiscale model for cardiovascular flows are (i) three-dimensional (3-D) fluid-structure interaction (FSI) models, which are used to represent few specific components of main interest, (ii) one-dimensional (1-D) FSI models, which describe the global blood circulation in the arterial network (see, e.g., Formaggia et al (2003), Alastruey et al (2007), Blanco et al (2011), and Malossi et al (2011a)), and (iii) lumped parameters models, which account for the cumulative effects of all distal vessels, i.e., small arteries, arterioles, and capillaries (see Formaggia et al (2009), Shi et al (2011), and references therein). More generally, from the medical point of view, a 3-D model allows

to have a deep insight of a specific region of the cardiovascular system (e.g., the thoracic aorta), whereas the interaction with the global cardiovascular system is modeled by the mean of reduced order models.

Despite the geometrical multiscale modeling idea is rather established, so far the greatest part of the existing literature has focused mainly on the mathematical and methodological aspects rather than on the application to patient-specific cardiovascular problems. In addition, at the best of our knowledge, evidences of the benefit of such a more complex model in respect to simplified problems, e.g., stand-alone 3-D FSI simulations, has been neither directly investigated nor quantified by numerical comparisons in real cardiovascular problems.

To fill this gap, in this work we provide several numerical comparisons of geometrical multiscale models with the aim of proving, and somehow quantifying, the benefits of such complex dimensionally-heterogeneous problems in respect to other simpler approaches. The geometrical multiscale models are set up by coupling one or more 3-D patient-specific geometries with a full network of 1-D models representing the global circulation of an average healthy patient. In particular, since the analysis of pathological scenarios is out of the scope of this work, we select two healthy 3-D geometries corresponding to the aorta and the iliac arteries of a patient. The results of these models are compared with both a full 1-D network of arteries and stand-alone 3-D FSI simulations, where the data at the inlet and outlet boundary interfaces are taken from a precomputed full 1-D network simulation. The comparisons are performed mainly in terms of flow rate and pressure wave forms. In addition, we also analyze the 3-D solid wall displacement magnitude.

On a slightly different context, we also focus on the calibration of cardiovascular simulations. Indeed, one critical aspect to get physiological results is the tuning of the problem parameters, especially for modeling 3-D FSI arteries. In this regard, it is essential to account for the correct boundary data on the the solid wall geometries. This problem has been already addressed in Crosetto et al (2011b) and Moireau et al (2012) for the external surface of the arterial wall, where Robin boundary conditions have been successfully used to account for the elastic and viscoelastic responses of the external tissues. Nevertheless, the values of the empiric tissue parameters appearing at the boundaries is rather difficult to estimate, and neither calibration procedures nor sensitivity analysis to show the effect of the variation of the parameters on the main quantities of interest were provided. Regarding the interface boundary rings of the arterial wall, in Formaggia et al (2007) and Malossi et al (2012) an approach to prescribe the continuity of the vessel area with surrounding models has been proposed. However, its impact on cardiovascular simulations compared to fixed area configurations has never been investigated, apart from few benchmark tests in simple geometries.

With the aim of covering the above mentioned aspects, in this work we also provide several comparisons and sensitivity analysis focused both on the calibration of the tissue parameters and on the analysis of the impact of different interface ring boundary conditions on the main quantities of interest.

This work is organized as follows. In Section 2 we describe the main ingredients of the geometrical multiscale approach. Then, in Section 3, we present the numerical results with several comparisons and sensitivity analyses. Finally, main conclusions are summarized in Section 4.

2 Geometrical multiscale approach

In this section we describe the main ingredients of the geometrical multiscale approach that we use to simulate the global arterial circulation. More precisely, we model the arterial network by coupling together different dimensionally-heterogeneous models, such as 3-D FSI models, which are used to represent specific components of main interest, 1-D FSI models, to simulate the pulse wave propagation in the global arterial system, and lumped parameters models, that accounts for the peripheral circulation. The latests correspond in general to well known simple differential algebraic equations, and for brevity are not detailed here. Finally, we briefly recall from other works the coupling equations and the numerical approach to solve the global network of models.

2.1 3-D FSI model for main arteries

In a geometrical multiscale setting, 3-D FSI models are used to simulate the hemodynamics in complex geometrical situations, such as those occurring at bifurcations, aneurysms, and stenoses among others. In addition, when patient-specific analyses are aimed for, the correct characterization of the local arterial flow has to be carried out by using patient-specific data obtained from 3-D medical images.

2.1.1 Equations

Let $\Omega \subset \mathbb{R}^3$ with boundary $\partial\Omega$, where $\bar{\Omega} = \bar{\Omega}_\mathrm{F} \cup \bar{\Omega}_\mathrm{S}$, being Ω_F and Ω_S the fluid and solid domains, respectively. In addition, let Γ_I be the fluid-solid interface $\partial\Omega_\mathrm{F} \cap \partial\Omega_\mathrm{S}$. The fluid-structure interaction problem employed in this work consists of the incompressible Navier–Stokes equations coupled with a linear elastic isotropic structure described by the St. Venant–Kirchhoff equations. To account for the interaction between the fluid and the solid, we define an Arbitrary

Lagrangian–Eulerian (ALE) map, i.e.,

$$\mathscr{M}^t : \Omega_{\mathrm{F}}^0 \to \Omega_{\mathrm{F}}^t \subset \mathbb{R}^3$$
$$x^0 \mapsto \mathscr{M}^t\left(x^0\right) = x^0 + d_{\mathrm{F}}\left(x^0\right),$$

where the superscripts 0 and t refer to the reference and current configurations, respectively (see Fig. 1), $x^0 \in \Omega_{\mathrm{F}}^0$ is a point, and d_{F} is the fluid domain displacement. More precisely, in this work we compute d_{F} as the harmonic extension of the solid displacement d_{S} at the reference fluid-solid interface Γ_{I}^0 to the interior of the reference fluid domain Ω_{F}^0.

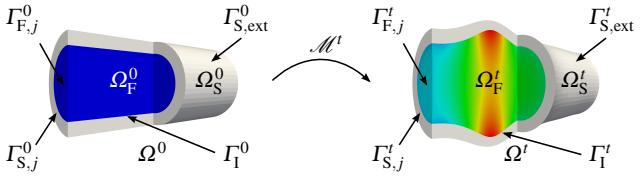

Figure 1: ALE map between reference and current configurations. The colors in the scheme refer to the computed pressure field.

The resulting FSI problem reads

$$\begin{cases} \left.\dfrac{\partial u_{\mathrm{F}}}{\partial t}\right|_{x^0} + \left(\left(u_{\mathrm{F}} - \left.\dfrac{\partial d_{\mathrm{F}}}{\partial t}\right|_{x^0}\right)\cdot\nabla\right) u_{\mathrm{F}} \\ \qquad -\dfrac{1}{\rho_{\mathrm{F}}}\nabla\cdot\sigma_{\mathrm{F}} = 0 \quad \text{in } \Omega_{\mathrm{F}}^t\times(0,T], \\ \qquad \nabla\cdot u_{\mathrm{F}} = 0 \quad \text{in } \Omega_{\mathrm{F}}^t\times(0,T], \\ \qquad \rho_{\mathrm{S}}\dfrac{\partial^2 d_{\mathrm{S}}}{\partial t^2} - \nabla\cdot\sigma_{\mathrm{S}} = 0 \quad \text{in } \Omega_{\mathrm{S}}^0\times(0,T], \\ \qquad -\Delta d_{\mathrm{F}} = 0 \quad \text{in } \Omega_{\mathrm{F}}^0\times(0,T], \\ \qquad u_{\mathrm{F}}\circ\mathscr{M}^t - \dfrac{\partial d_{\mathrm{S}}}{\partial t} = 0 \quad \text{on } \Gamma_{\mathrm{I}}^0\times(0,T], \\ \sigma_{\mathrm{S}}\cdot n_{\mathrm{S}} - J_{\mathrm{S}}\mathrm{G}_{\mathrm{S}}^{-\mathsf{T}}\left(\sigma_{\mathrm{F}}\circ\mathscr{M}^t\right)\cdot n_{\mathrm{S}} = 0 \quad \text{on } \Gamma_{\mathrm{I}}^0\times(0,T], \\ \qquad d_{\mathrm{F}} - d_{\mathrm{S}} = 0 \quad \text{on } \Gamma_{\mathrm{I}}^0\times(0,T], \end{cases} \tag{1}$$

where $(0,T]$ is the time interval, u_{F} the fluid velocity, ρ_{F} and ρ_{S} are the fluid and solid density, respectively, n_{S} is the outgoing normal direction applied to the solid domain, $\mathrm{G}_{\mathrm{S}} = \mathrm{I} + \nabla d_{\mathrm{S}}$ the solid deformation gradient (with I the identity matrix), and $J_{\mathrm{S}} = \det\left(\mathrm{G}_{\mathrm{S}}\right)$. In addition, σ_{F} and σ_{S} are the Cauchy and the first Piola–Kirchhoff stress tensors, respectively, i.e.,

$$\sigma_{\mathrm{F}} = -p_{\mathrm{F}}\mathrm{I} + 2\mu_{\mathrm{F}}\,\varepsilon_{\mathrm{F}}\left(u_{\mathrm{F}}\right),$$
$$\sigma_{\mathrm{S}} = \lambda_{\mathrm{S}}(E_{\mathrm{S}},\nu_{\mathrm{S}})\mathrm{tr}\left(\varepsilon_{\mathrm{S}}\left(d_{\mathrm{S}}\right)\right)\mathrm{I} + 2\mu_{\mathrm{S}}(E_{\mathrm{S}},\nu_{\mathrm{S}})\varepsilon_{\mathrm{S}}\left(d_{\mathrm{S}}\right),$$

where $\varepsilon_{\mathrm{F}}\left(u_{\mathrm{F}}\right)$ is the strain rate tensor, being p_{F} the fluid pressure and μ_{F} the fluid dynamic viscosity, and $\varepsilon_{\mathrm{S}}\left(d_{\mathrm{S}}\right)$ is the linear strain tensor, being λ_{S} and μ_{S} the first and second Lamé parameters, respectively, which are algebraic functions of the Young modulus E_{S} and the Poisson coefficient ν_{S} of the wall material.

Problem (1) is closed by a proper set of initial and boundary conditions. More precisely, on the external wall $\Gamma_{\mathrm{S,ext}}^0$ we apply a viscoelastic Robin boundary condition to account for the presence of the external tissues, as we detail in Section 2.1.3. On $\Gamma_{\mathrm{F},j}^t \subset \partial\Omega_{\mathrm{F}}^t \backslash \Gamma_{\mathrm{I}}^t$, $j = 1,\ldots,n_{\mathrm{FS}}^{\Gamma}$ we impose either inflow and outflow boundary data or continuity equations with the surrounding models, which are detailed in Section 2.3. Similarly, the inlet/outlet solid rings $\Gamma_{\mathrm{S},j}^0$, $j = 1,\ldots,n_{\mathrm{FS}}^{\Gamma}$ can be either fixed or scaled to match the area of surrounding models, as described in Malossi et al (2012) and briefly recalled in Section 2.3.

Remark 1 Several models of the arterial wall are described in literature, with different levels of complexity (see, e.g., Fung (1993), Holzapfel et al (2000), and Holzapfel and Ogden (2006)). An accurate model for the arterial wall should take into account the effects of anisotropy due to the distribution of the collagen fibers, the three layers (intima, media and adventitia) structure, the nonlinear behavior due to collagen activation, and the incompressibility constraint. Nevertheless, a linear elastic isotropic structure is still considered a reasonable approximation for the large healthy arteries, as demonstrated numerically in, e.g., Crosetto et al (2011b) and Crosetto et al (2012), and validated experimentally in, e.g., Kanyanta et al (2009).

2.1.2 Numerical approximation

The FSI problem is solved by using a non-modular (monolithic) approach, whose details are given in Crosetto (2011) and Crosetto et al (2011a). The fluid problem is discretized in space by a $\mathbb{P}1$–$\mathbb{P}1$ finite element method, stabilized by an interior penalty technique (see Burman et al (2006)). The solid and the geometric problems are discretized in space by $\mathbb{P}1$ finite elements. Regarding time discretizations for the incompressible Navier–Stokes equations on moving domains we use a first order Euler scheme, while for the structural problem we use an explicit second order mid-point scheme. The time interval $[0,T]$ is split into subintervals $[t^n, t^{n+1}]$, $n = 0,1,2,\ldots$, such that $t^n = n\Delta t$, Δt being the time step. The fluid and solid problems are coupled by using the geometric convective explicit time discretization, i.e., the fluid problem is linearized by considering explicit the fluid domain displacement and the convective term. This choice allows to split the solution of the geometric part (the harmonic extension) from the fluid-solid one, leading to a significant reduction of the computational cost. For more details on the 3-D FSI problem see Crosetto (2011) and Crosetto et al (2011a).

2.1.3 Robin boundary condition for the solid external wall

From the modeling point of view, one critical aspect to get physiological results in a 3-D FSI simulation is the tuning of the boundary condition on the solid external wall. The influence of external tissues and organs tethering and constraining the movement of blood vessels is of critical importance when simulating 3-D FSI problems in the arterial system (see, e.g., Liu et al (2007)). At the present time, the modeling of the detailed multi-contact relations between the arteries and the other tissues is unfeasible. However, Crosetto et al (2011b) show that for 3-D FSI problems the elastic behavior of external tissues support on the outer arterial wall can be handled by enforcing a Robin boundary condition on $\Gamma^0_{S,ext}$. This approach has been further extended in Moireau et al (2012) to include also the viscoelastic response of the tissues, such that the resulting Robin boundary condition for the 3-D FSI problem reads

$$\sigma_S \cdot n_S + k_S d_S + c_S v_S + P_{ext} n_S = 0, \quad \text{on } \Gamma^0_{S,ext} \times (0,T], \quad (2)$$

where v_S is the velocity of the solid domain and P_{ext} the reference external pressure. The parameters k_S and c_S account for the elastic and viscoelastic response of the external tissues, respectively. More generally, they are empiric coefficients that depend on space and, possibly, on time (e.g., to represent the change of mechanical properties over time).

Tuning the value of the parameters k_S and c_S is rather difficult. In both Crosetto et al (2011b) and Moireau et al (2012) a range of orders of magnitude for the aorta is identified on the basis of qualitative considerations about the pulse wave velocity and the maximum admissible displacement of the vessel wall. However, neither further investigations nor sensitivity analyses that show the effect of the variation of the parameters on the main quantities of interest are provided. To fill this gap, in Sections 3.3.1 and 3.3.2 we perform several comparisons in terms of flow rate and displacement for the aorta and iliac arteries, respectively, as a function of different sets of values for the parameters k_S and c_S.

Remark 2 From the numerical viewpoint, the Robin boundary condition must be implemented according to the time discretization scheme used in the solid problem. In particular, since in this work we use an explicit second order midpoint scheme, the following relation holds

$$\frac{v_S^{n+1} + v_S^n}{2} = \frac{d_S^{n+1} - d_S^n}{\Delta t},$$

such that, for $n = 0, 1, 2, \ldots$, the discrete form of (2) reads

$$\sigma_S \cdot n_S + \left(k_S + c_S \frac{2}{\Delta t}\right) d_S^{n+1} - \left(\frac{2c_S}{\Delta t} d_S^n + c_S v_S^n\right) + P_{ext} n_S = 0, \quad \text{on } \Gamma^0_{S,ext}.$$

2.2 1-D FSI model for the global arterial circulation

In a geometrical multiscale setting, the global arterial circulation can be modeled by a network of 1-D FSI models. Despite its simple axial symmetric representation of the blood flow, it has proven to be able to provide accurate information under physiological and pathophysiological conditions, and therefore gives insight about the main characteristics that lead to the interplay among physical phenomena taking place in the systemic arteries.

2.2.1 Equations

The 1-D FSI model is derived from the incompressible Navier–Stokes equations by introducing some simplifying hypotheses on the behavior of the flow quantities over the cross-section of the artery. The structural model is accounted through a simple pressure-area relation. Being $z \in [0, L]$ the axial coordinate, with L the length of the vessel, the resulting governing equations are

$$\begin{cases} \dfrac{\partial A}{\partial t} + \dfrac{\partial Q}{\partial z} = 0 & \text{in } (0,L) \times (0,T], \\ \dfrac{\partial Q}{\partial t} + \dfrac{\partial}{\partial z}\left(\alpha_F \dfrac{Q^2}{A}\right) + \dfrac{A}{\rho_F}\dfrac{\partial P}{\partial z} + \kappa_F \dfrac{Q}{A} = 0 & \text{in } (0,L) \times (0,T], \\ P - \psi(A) = 0 & \text{in } (0,L) \times (0,T], \end{cases} \quad (3)$$

where α_F and κ_F are the Coriolis and friction coefficients, respectively, whose definitions are given in Malossi et al (2011a), A is the cross-sectional area, Q the volumetric flow rate, P the average pressure, and

$$\psi(A) = P_{ext} + \beta_S \left(\sqrt{\frac{A}{A^0}} - 1\right) + \gamma_S \left(\frac{1}{A\sqrt{A}} \frac{\partial A}{\partial t}\right), \quad (4)$$

where

$$\beta_S = \sqrt{\frac{\pi}{A_0}} \frac{h_S E_S}{1 - \nu_S^2}, \qquad \gamma_S = \frac{T_S \tan \phi_S}{4\sqrt{\pi}} \frac{h_S E_S}{1 - \nu_S^2},$$

being A^0 the reference value for the vessel area, h_S the wall thickness, T_S the wave characteristic time, and ϕ_S the viscoelastic angle. The second and third terms in (4) account for the elastic and viscoelastic response of the vessel wall.

Problem (3) is finally closed by a proper set of initial and boundary conditions. The latter can be either inflow and outflow boundary data or continuity equations with the surrounding models, as we detail in Section 2.3.

2.2.2 Numerical approximation

The 1-D FSI problem is solved by using an operator splitting technique based on an explicit second order Taylor–Galerkin discretization, where the solution of the problem is split into two steps, such that the first one corresponds to the solution of a purely elastic problem, while the second one provides a viscoelastic correction. The spatial discretization is accomplished using $\mathbb{P}1$ finite elements. For more details see Malossi et al (2011a) and references therein.

2.3 Interface equations for the global network of models

The solution of the global dimensionally-heterogeneous problem is addressed following the approach first devised in Malossi et al (2011b) and later extended in Malossi et al (2012) to account for the continuity of the vessel area. More precisely, let us consider a general network of heterogeneous models connected by $\mathscr{C}$ coupling nodes. At each node we write the conservation of averaged/integrated quantities over the interfaces, such that the interface problem does not have any dependency on the geometrical nature nor on the mathematical formulation of each model. More specifically, these boundary quantities are the volumetric flow rate $\mathcal{Q}$, the averaged normal component of the traction vector $\mathcal{S}$, and the area of the fluid section $\mathcal{A}$, hereafter referred to as *coupling flow*, *coupling stress*, and *coupling area*, respectively. On the jth coupling interface of the 3-D FSI model these quantities are computed as

$$\mathcal{Q}_j^{\text{3-D}} = \int_{\Gamma_{\text{F},j}^t} u_{\text{F}} \cdot n_{\text{F}} \, \mathrm{d}\Gamma, \quad \mathcal{S}_j^{\text{3-D}} = \frac{1}{\left|\Gamma_{\text{F},j}^t\right|} \int_{\Gamma_{\text{F},j}^t} (\sigma_{\text{F}} \cdot n_{\text{F}}) \cdot n_{\text{F}} \, \mathrm{d}\Gamma,$$
$$\mathcal{A}_j^{\text{3-D}} = \left|\Gamma_{\text{F},j}^t\right|, \qquad j = 1, \dots, n_{\text{FS}}^{\Gamma},$$

where n_{F} is the outgoing normal direction applied to the fluid domain. The 3-D FSI fluid problem is closed by imposing $(\sigma_{\text{F}} \cdot n_{\text{F}}) \cdot \tau_{2\text{F}} = 0$ and $(\sigma_{\text{F}} \cdot n_{\text{F}}) \cdot \tau_{2\text{F}} = 0$ on $\Gamma_{\text{F},j}^t$, $j = 1, \dots, n_{\text{FS}}^{\Gamma}$, where $\tau_{1\text{F}}$ and $\tau_{2\text{F}}$ are the two tangential directions. In addition, we assume that the normal stress $(\sigma_{\text{F}} \cdot n_{\text{F}}) \cdot n_{\text{F}}$ is constant over the coupling interfaces. Regarding the solid problem, the vessel area is imposed by prescribing a radial displacement of the internal contour of the jth 3-D solid ring, i.e.,

$$\begin{cases} d_{\text{S}} \cdot n_{\text{S}} = 0 & \text{on } \Gamma_{\text{I}}^0 \cap \Gamma_{\text{S},j}^0 \times (0,T], \\ \left[d_{\text{S}} - \Psi_j^t \left(x^0 - x_{\text{G},j}^0 \right) \right] \cdot \tau_{1\text{S}} = 0 & \text{on } \Gamma_{\text{I}}^0 \cap \Gamma_{\text{S},j}^0 \times (0,T], \\ \left[d_{\text{S}} - \Psi_j^t \left(x^0 - x_{\text{G},j}^0 \right) \right] \cdot \tau_{2\text{S}} = 0 & \text{on } \Gamma_{\text{I}}^0 \cap \Gamma_{\text{S},j}^0 \times (0,T], \end{cases}$$

for $j = 1, \dots, n_{\text{FS}}^{\Gamma}$, where $\tau_{1\text{S}}$ and $\tau_{2\text{S}}$ are the two tangential directions lying on $\Gamma_{\text{S},j}^0$, $j = 1, \dots, n_{\text{FS}}^{\Gamma}$. This corresponds to scale the boundary area preserving its original shape, where the radial scale factor is defined as

$$\Psi_j^t = \sqrt{\frac{\mathcal{A}_j^{\text{3-D}}}{A_j^0}} - 1,$$

being A_j^0 and $x_{\text{G},j}^0$ the reference area of the jth coupling interface of the 3-D fluid problem and its geometric center, respectively. Note that to close the 3-D FSI solid problem, we need to impose an additional boundary condition on $\Gamma_{\text{S},j}^0 \setminus \Gamma_{\text{I}}^0 \cap \Gamma_{\text{S},j}^0$, $j = 1, \dots, n_{\text{FS}}^{\Gamma}$, which in our case is $\sigma_{\text{S}} \cdot n_{\text{S}} = 0$. Regarding the two coupling interfaces of the 1-D FSI model we have

$$\mathcal{Q}_{\text{L}}^{\text{1-D}} = -Q_{\text{L}}, \qquad \mathcal{S}_{\text{L}}^{\text{1-D}} = -P_{\text{L}}, \qquad \mathcal{A}_{\text{L}}^{\text{1-D}} = A_{\text{L}},$$
$$\mathcal{Q}_{\text{R}}^{\text{1-D}} = Q_{\text{R}}, \qquad \mathcal{S}_{\text{R}}^{\text{1-D}} = -P_{\text{R}}, \qquad \mathcal{A}_{\text{R}}^{\text{1-D}} = A_{\text{R}},$$

where the subscripts L and R stand for left and right quantities, respectively.

The resulting set of conservation equations for the fluid part of the interface problem is

$$\begin{cases} \displaystyle\sum_{i=1}^{\mathscr{I}_c} \mathcal{Q}_{c,i} = 0, \\ \mathcal{S}_{c,1} - \mathcal{S}_{c,i} = 0, \quad i = 2, \dots, \mathscr{I}_c, \end{cases} \tag{5}$$

where $\mathscr{I}_c$ is the number of interfaces connected by the cth coupling node, $c = 1, \dots, \mathscr{C}$. More precisely, the first equation ensures the conservation of the mass and the second implies the continuity of the mean normal stress. In case the continuity of the vessel area is enforced between two vessels, the set of equations (5) becomes

$$\begin{cases} \mathcal{Q}_{c,1}^{\text{1-D}} + \mathcal{Q}_{c,2}^{\text{3-D}} = 0, \\ \mathcal{S}_{c,1}^{\text{1-D}} - \mathcal{S}_{c,2}^{\text{3-D}} = 0, \\ \mathcal{A}_{c,1}^{\text{1-D}} - \mathcal{A}_{c,2}^{\text{3-D}} = 0, \end{cases} \tag{6}$$

where, for the sake of clarity, the model to which each quantity belongs is indicated in the superscript. More precisely, the continuity of the vessel area cannot be imposed between two 1-D FSI vessels. In fact, due to modeling reasons, the 1-D FSI problem needs just one physical boundary condition on each side of the segment, and therefore it is not possible to impose both a fluid quantity and the vessel area at the same time. On the contrary, the 3-D FSI model needs boundary data on both the fluid and the solid parts of each interface, such that it is possible to set the continuity of its boundary areas with the surrounding 1-D FSI models. In addition, we remark that (6) is written for the specific case of a 3-D FSI interface coupled with a single 1-D FSI model. In the case of a generalization to two or more 1-D models connected to the same 3-D FSI interface, the continuity of

the area does not make sense, and for this reason we do not address this case. For more details see Malossi et al (2012).

From the numerical viewpoint, the global interface problem is written in a residual formulation and solved by Newton or inexact-Newton approaches, where the Jacobian matrix is either computed analytically, by solving the tangent problem associated to each model, or approximated with finite differences. To avoid the recomputation of the Jacobian matrix at each iteration, a Broyden method can also be used. For more details on the interface problem see Malossi et al (2011a), Malossi et al (2011b), and Malossi et al (2012).

3 Numerical simulations

In this section we present several comparisons among different geometrical multiscale models. The purpose of these comparisons is manifold. On the one hand, we study the interaction between 3-D patient specific geometries and a global arterial network of 1-D models. This results are compared both with a full 1-D network of arteries, and a standalone 3-D simulation with boundary data taken from the same full 1-D network. On the other hand, we also analyze the effect of the 3-D solid boundary conditions on the simulations. In particular, we perform a sensitivity analysis of the external tissues parameters, and we also compare results of configurations where the area at the interfaces is fixed, with those where it is scaled to have the continuity of the vessels size with the surrounding 1-D arteries.

3.1 Human arterial tree model

To model the global circulation we use the data of the arterial network provided in Reymond et al (2009, Fig. 2 and Table 2), which is composed by 103 elements (4 coronary, 24 aortic, 51 cerebral, 10 upper limbs, and 14 lower limbs) and includes all the values of the parameters required to describe the blood flow, such as the geometrical properties of the vessels (length and proximal/distal areas) and the data for the terminals, which are modeled as three-element windkessel elements and account for the cumulative effects of all distal vessels (small arteries, arterioles, and capillaries). These values have been obtained both from *in vivo* measurements and averaged literature data. The presence of the venous circulation is taken into account by imposing the return venous pressure P_v on the distal side of each windkessel terminal. Regarding the parameters of the wall, since we use a different model, we estimate these values from other sources, as fully described in Malossi et al (2011a). The main parameters that define the problem are summarized in Table 1.

Table 1: Main parameters of the 1-D network of arteries. For more details see Malossi et al (2011a) and references therein.

ρ_F	Fluid density	1.04	g/cm^3
μ_F	Fluid viscosity	0.035	g/cm/s
κ_F	Friction coefficient	2.326	cm^2/s
α_F	Coriolis coefficient	1.1	
P_{ext}	Reference external pressure	100000	dyn/cm^2
P_v	Venous pressure	6666	dyn/cm^2
h_S/R_S	Solid thickness/ local radius	0.1	
E_S	Young modulus	$3 - 12 \cdot 10^6$	dyn/cm^2
ν_S	Poisson coefficient	0.50	
ϕ_S	Viscoelastic angle	10	degree
T_S	Systolic period	0.24	s
	Heart rate	75	bpm

3.2 Geometry reconstruction and mesh generation

In this work we use the 3-D FSI model to simulate the flow in two main patient-specific arteries, i.e., the aorta and the iliac of an healthy patient. These geometries have several bifurcations and some severe bends, such that the 3-D dynamics of the blood is not negligible.

The segmentation of the arterial geometries were obtained through MRI Time of Flight acquisition on a 3T MRI scanner (Siemens Trio-Tim 3T System); details on the used sequences are given in Reymond et al (2011). Then, the arterial geometries were reconstructed in 3-D from MRI magnitude data (ITK Snap software). Since the thickness of the wall is not visible in MRI data, it has to be synthetically reconstructed. In particular, it has been estimated equal to 10 percent of local lumen radius, which is a commonly accepted approximation (see, e.g., Langewouters (1982)).

To correctly model the different material properties of the arterial wall and of the external tissues, we divide the solid domain into several regions, which are schematically shown in Fig. 2. Note that for the iliac geometry we provide two different configurations, which are later used in Section 3.3.2 for a numerical comparison of the results as a function of the tissue parameters at the bifurcations. The main wall parameters that define the 3-D problems are summarized in Table 2.

Table 2: Wall parameters of the 3-D FSI arteries. The Young modulus of the 3-D FSI aorta and iliac is 3000000 dyn/cm^2 in all the branches apart from the vertebral arteries, where it is 6000000 dyn/cm^2, and inner iliac arteries, where it is 12000000 dyn/cm^2.

ρ_S	Wall density	1.2	g/cm^3
h_S/R_S	Wall thickness / local radius	0.1	
E_S	Young modulus	$3 - 12 \cdot 10^6$	dyn/cm^2
ν_S	Poisson coefficient	0.48	

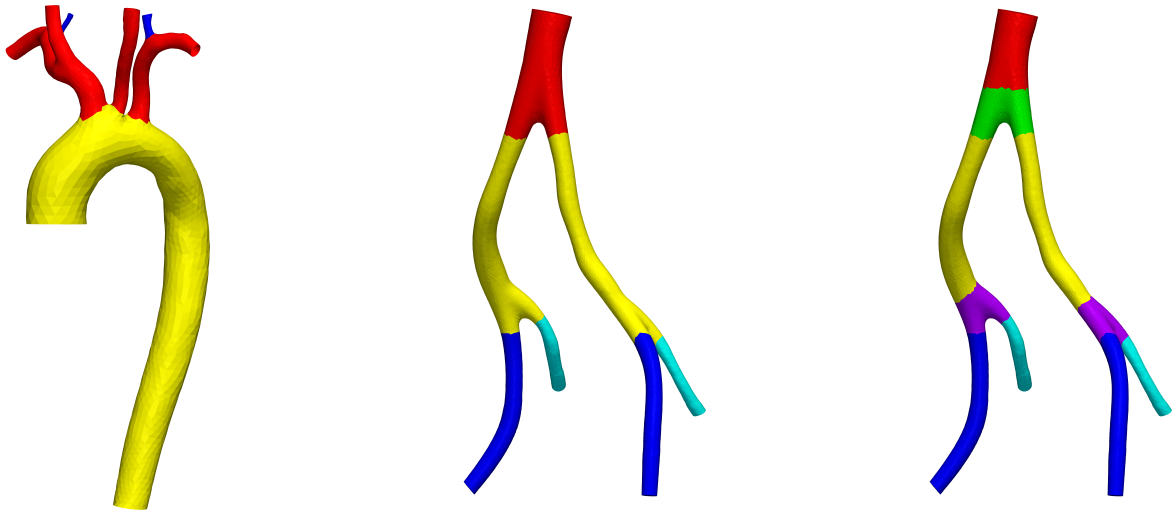

(a) (b) (c)

Figure 2: View of the aorta and iliac geometries with wall regions. (a) The aorta is divided in three regions: aortic arch (yellow), carotids and subclavians (red), and vertebrals (blue). (b) The iliac is divided in four regions: abdominal aorta (red), common iliac (yellow), external iliac (blue), and inner iliac (ciano). (c) Same as (b) with two additional regions at the bifurcations: abdominal aorta bifurcation (green) and common iliac bifurcations (magenta).

Finally, for each arterial vessel two separate conforming fluid and solid geometries have been generated using the VTK[1], VMTK[2], and ITK[3] libraries, as detailed in Bonnemain et al (2012). The resulting mesh of the fluid part of the 3-D aorta consists of 280199 unstructured tetrahedral elements with 50866 vertices, while the solid part is made of 278904 structured tetrahedral elements with 58565 vertices. The corresponding average space discretizations for both the fluid and solid problems is 0.158 cm. Regarding the 3-D iliac, the mesh of the fluid part consists of 350376 unstructured tetrahedral elements with 63716 vertices, while the solid part is made of 359256 structured tetrahedral elements with 60788 vertices. In this case, the corresponding average space discretizations for both the fluid and solid problems is 0.076 cm. All the simulations presented in this work have been performed on several cluster nodes with two Intel® Xeon® processors X5550 (quad core, 8 MB cache, 2.66 GHz CPU) each, interconnected by a 20 Gb/s InfiniBand® architecture.

3.3 Geometrical multiscale modeling

In this section we set up three different geometrical multiscale models where the 3-D patient-specific vessels in Fig. 2 are embedded in the 1-D network described in Section 3.1, which represents an average healthy patient. To set up the models we use the following procedure. First of all, we identify the 1-D elements of the network to be removed or cut, since they overlap with some regions of the 3-D patient-specific geometries. This is done by measuring the length of the different branches of the 3-D vessels and comparing these data with the one of the 1-D network. Obviously, this phase presents several degrees of freedom and arbitrariness. The degree of precision of this step also depends on the region of interest and the required level of accuracy (e.g., rough evaluation of flow versus precise local quantification for surgery planning). In a clinical context this operation should be supervised by the clinician in order to immediately determine the crucial regions for the numerical simulations. Once the 1-D elements are cut, the second step consists in changing the reference area and the wall thickness of the 1-D arteries in order to match the one of the nearby 3-D interfaces. Since the 3-D geometries are not symmetric, it is possible that some asymmetries are introduced also in the 1-D networks (e.g., between the left and right external iliac arteries). Moreover, it is important to check that the resulting distal area is always smaller or equal than the proximal one. If it is not the case, some further adjustments to the 1-D elements are required to avoid a non-physiological behavior of the flow in those elements.

[1] www.vtk.org
[2] www.vmtk.org
[3] www.itk.org

Table 3: Empiric external tissues coefficients at the different wall regions of the 3-D aorta (see Fig. 2a). We define five cases for the sets of values of the elastic coefficient.

Artery	k_S [dyn/cm^3]					c_S [dyn s/cm^3]
	E_1^A	E_2^A	E_3^A	E_4^A	E_5^A	
Aortic arch	15000	30000	45000	60000	75000	0.0
Left / right carotid and subclavian	22500	45000	67500	90000	112500	0.0
Left / right vertebral	30000	60000	90000	120000	150000	0.0

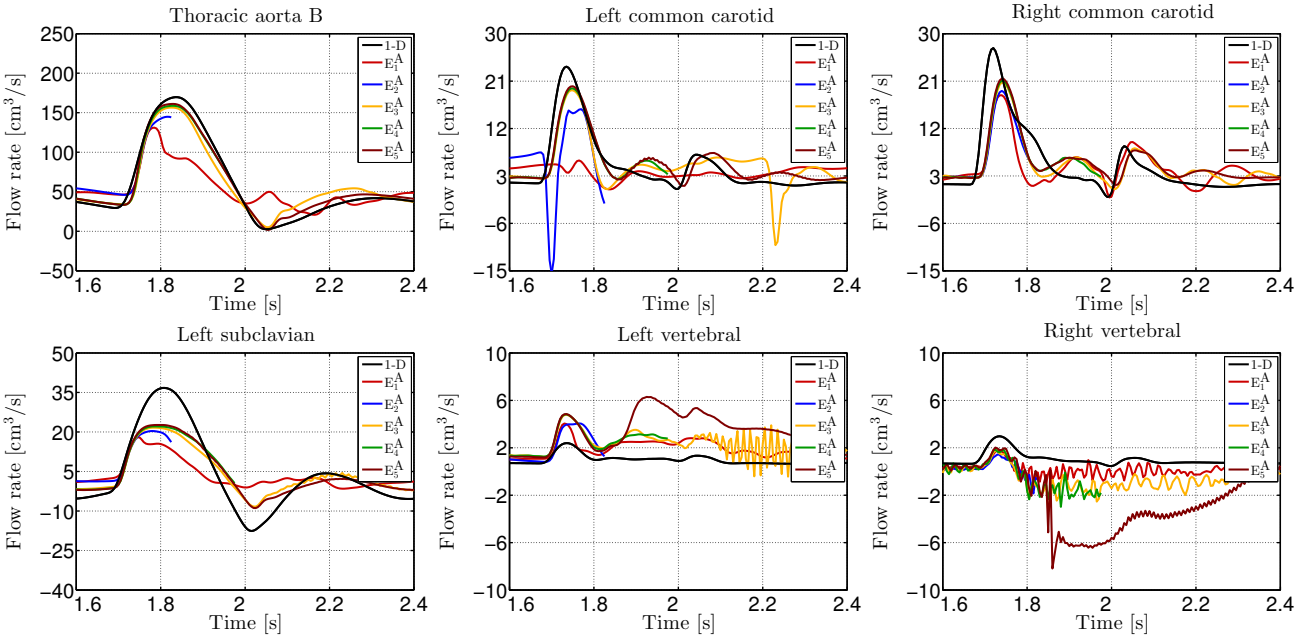

Figure 3: Flow rate comparison, at the third heart beat, for the sets of values given in Table 3 (elastic behavior of the external tissues), at the most significant coupling interfaces between the 3-D aorta (see Fig. 2a) and the 1-D network. The black line is the solution of the full 1-D network.

3.3.1 External tissues parameters comparisons: 3-D aorta

In this section we focus on the study of the external tissues parameters k_S and c_S introduced by the Robin boundary condition on the arterial wall of the 3-D FSI problem. For this analysis, we consider a geometrical multiscale model assembled by coupling the 3-D patient-specific aorta in Fig. 2a with the 1-D arterial tree described in Section 3.1, which represents an average healthy patient. For the sake of simplicity, the results presented in this section are obtained by fixing the position of the boundary solid rings of the 3-D arterial wall of the aorta, i.e., $d_S = 0$ on $\Gamma^0_{S,j}, j = 1, \ldots, n^{\Gamma}_{FS}$.

The first study we perform consists in a sensitivity analysis of the main quantities of interest in respect to a variation of the elastic parameter k_S. This is done by assuming $c_S = 0$ dyn s/cm^3 and choosing five sets of values for the coefficient k_S at the different branches of the aorta, as detailed in Table 3. Note that the values of the different cases are chosen as multiples of the ones of case E_1^A.

The results of this comparison, at the most significant coupling interfaces between the 3-D aorta and the 1-D network, are summarized in Fig. 3. First of all, we observe that the behavior of the flow rate is quite different in each of the five considered cases. In addition, some spurious oscillations are always present. More precisely, the tissues of case E_1^A are not stiff enough to correctly represent the wave propagation even in the thoracic aorta B interface. Case E_2^A and E_4^A fail to compute the solution of the problem during the third heat beat, due to some numerical instabilities in the simulated flow. Case E_3^A still presents some non-physical high-frequency oscillations at most of the coupling interfaces, while case E_5^A, whose tissues are the stiffest one, behaves better than the others, however it still leads to strong spurious high-frequency oscillations at the right vertebral interface. Moreover, the comparison of the displacement magnitude field of the 3-D arterial wall of the aorta at the second heart beat (see Fig. 4) shows that the first three set of values in Table 3 are not stiff enough to prevent the overinflation of

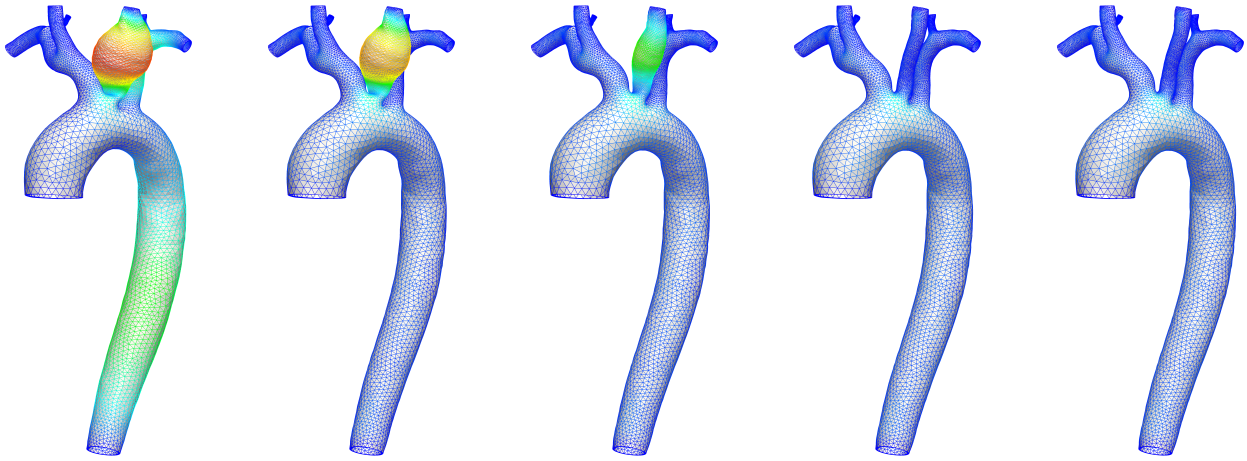

Case E_1^A. Case E_2^A. Case E_3^A. Case E_4^A. Case E_5^A.

Figure 4: Wall displacement magnitude comparison, at the end-systole of the second heart beat ($t = 1.2$ s), for the sets of values given in Table 3 (elastic behavior of the external tissues) of the 3-D aorta (see Fig. 2a) coupled with the 1-D network (not shown). The color bar ranges from blue (0.0 cm) to red (1.8 cm).

the left common carotid artery. In view of these preliminary results, we can conclude that a purely elastic Robin boundary condition on the arterial wall of the 3-D FSI models is not adequate to model the physical behavior of the flow. In particular, none of the presented cases leads to the correct wave propagation in the aortic branches.

Since the results with a purely elastic Robin boundary condition are not satisfactory, for the second analysis we introduce the viscoelastic response of the tissues through the parameter c_S. As previously done for the elastic parameter, also in this case we select several sets of values for the coefficient c_S at the different branches of the aorta, as detailed in Table 4. Regarding the elastic parameter, we chose the set of values E_4^A, which has proven to be stiff enough to prevent overinflations in all the branches of the 3-D geometry.

The results of this comparison, at the same interfaces of the previous one, are summarized in Fig. 5. First of all, we observe that the spurious high-frequency oscillations disappear at all the boundary interfaces and independently from the chosen set of values for the parameter c_S. This behavior confirms the importance of including the viscoelastic effects in the model of the arterial wall, not only in 1-D FSI simulations, as already proven, for instance, in Malossi et al (2011a), but also in 3-D FSI problems, as claimed in Moireau et al (2012). Regarding the value of the viscoelastic parameter, we observe that the flow rate wave forms change significantly among the simulated cases. More precisely, the set of values V_1^A and V_2^A, are not high enough to smooth the low-frequency oscillations of the 3-D FSI elastic wall. On the contrary, the results given by the other four sets of values are all very similar and belong to the physiological regime. In particular, we observe a sort of limit behavior of the viscoelastic parameter, such that above a certain threshold the sensitivity of the flow rate wave form to a variation of the parameter c_S becomes very small. In view of these results, hereafter we compute the value of the viscoelastic parameter as one tenth of the value of the corresponding elastic one. This rule provides a reliable and easy way to calibrate the viscoelastic parameter of the Robin boundary condition for the external tissues.

3.3.2 External tissues parameters comparisons: 3-D iliac

In this section we further extend the study of the external tissues parameters k_S and c_S by considering a different problem. More precisely, we set up a geometrical multiscale model composed by the 3-D patient-specific iliac in Fig. 2b coupled with the 1-D arterial tree described in Section 3.1, which represents an average healthy patient. For the sake of simplicity, the results presented in this section are obtained by fixing the position of the boundary solid rings of the 3-D arterial wall of the iliac, i.e., $d_S = 0$ on $\Gamma^0_{S,j}, j = 1, \ldots, n^{\Gamma}_{FS}$.

First of all, we perform a sensitivity analysis of the main quantities of interest in respect to a variation of the external tissues parameters. In view of the results achieved in the previous section, we directly consider both the elastic and viscoelastic coefficients. For the first one, we choose five sets of values at the different branches of the iliac, as detailed in Table 5. Note that the values of the different cases are chosen as multiples of the ones of case E_1^I. Then, following the

Table 4: Empiric external tissues coefficients at the different wall regions of the 3-D aorta (see Fig. 2a). We define six cases for the sets of values of the viscoelastic coefficient.

Artery	k_S [dyn/cm^3]	c_S [dyn s/cm^3]					
	E_4^A	V_1^A	V_2^A	V_3^A	V_4^A	V_5^A	V_6^A
Aortic arch	60000	500	1000	5000	10000	50000	100000
Left / right carotid and subclavian	90000	500	1000	5000	10000	50000	100000
Left / right vertebral	120000	500	1000	5000	10000	50000	100000

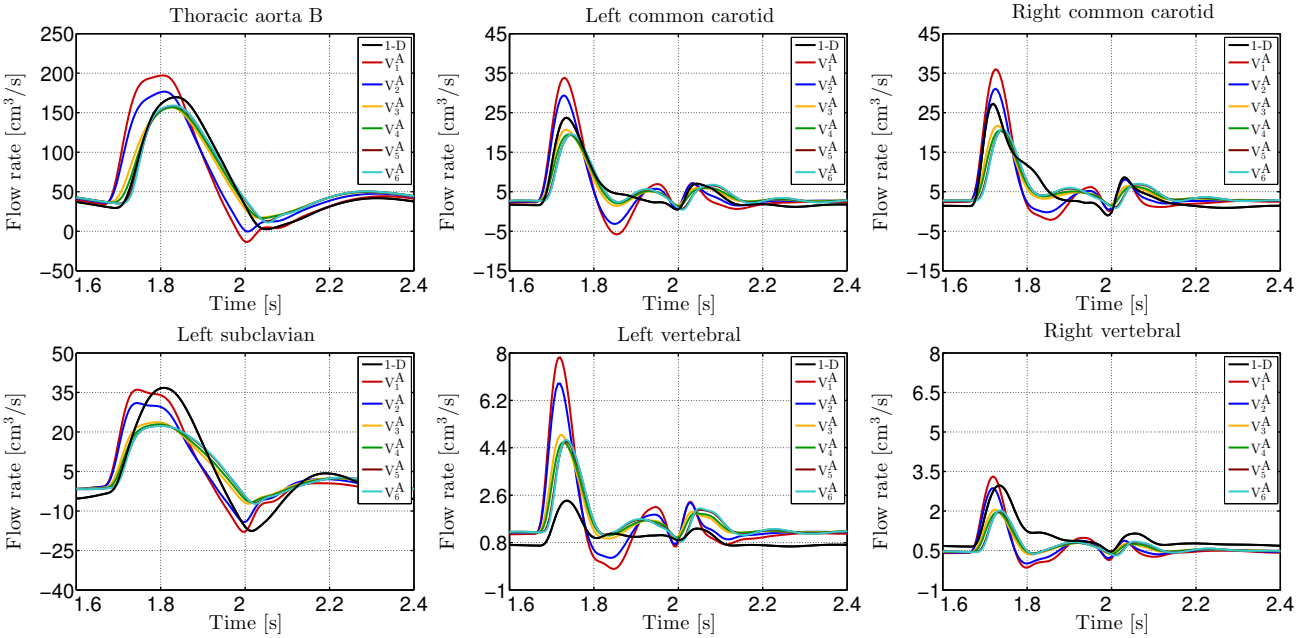

Figure 5: Flow rate comparison, at the third heart beat, for the sets of values given in Table 4 (elastic and viscoelastic behavior of the external tissues), at the most significant coupling interfaces between the 3-D aorta (see Fig. 2a) and the 1-D network. The black line is the solution of the full 1-D network.

result of the previous section, the viscoelastic parameter is obtained from the relation: $c_S = k_S/10$.

The results of this comparison, at the most significant coupling interfaces between the 3-D iliac and the 1-D network, are summarized in Fig. 6. From the images we observe that, apart from case E_1^I, whose tissues are clearly not stiff enough, all the other cases lead to results in a physiological regime. Moreover, there are no significant differences among the last four cases, even if the parameters change considerably. In view of these results we can conclude that, above a certain threshold, the sensitivity of the flow rate wave form to a variation of the external tissues parameters is very small when considering both the elastic and viscoelastic components. In particular, we remark that the high sensitivity observed in Fig. 3 for the aorta was mainly due to the numerical instabilities and, consequently, to the high-frequency oscillations in the solution, rather than to a true sensitivity to the elastic parameter k_S.

Regarding the displacement of the 3-D arterial wall, similarly to the previous section, we observe a gradual decrease in the displacement magnitude in respect to an increase in the value of the tissues parameters. No overinflations appear along the iliac branches, in all the simulated cases. However, even in the stiffest case, we observe some severe overinflations at all the three bifurcations. This non-physiological behavior is due to the lack of collagen fibers in the arterial wall model, which consequently becomes weaker at the branching points.

To solve this issue without introducing a more complex model for the 3-D vessel wall, we use a second configuration of the iliac geometry, where two additional regions are introduced at the bifurcations (see Fig. 2c). Then we choose case E_4^I as the reference one, and we introduce three additional sets of values for the tissues parameters at the iliac bifurcations, as detailed in Table 6. As before, the values of the different cases are chosen as multiples of the reference one.

Table 5: Empiric external tissues coefficients at the different wall regions of the 3-D iliac (see Fig. 2b). We define five cases for the sets of values of the coefficients.

Artery	k_S [dyn/cm^3]					c_S [dyn s/cm^3]
	E_1^I	E_2^I	E_3^I	E_4^I	E_5^I	
Abdominal aorta	25000	50000	75000	100000	125000	$k_S/10$
Left / right common iliac	35000	70000	105000	140000	112500	$k_S/10$
Left / right external iliac	37500	75000	112500	150000	187500	$k_S/10$
Left / right inner iliac	42500	85000	127500	170000	212500	$k_S/10$

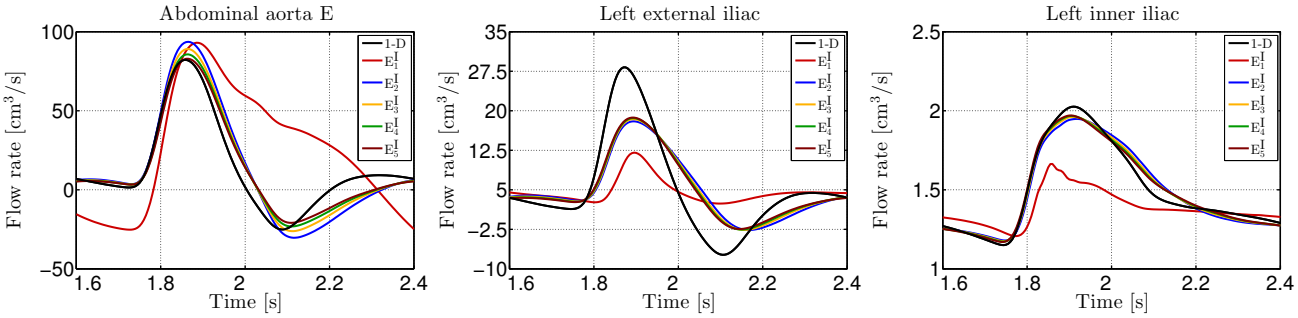

Figure 6: Flow rate comparison, at the third heart beat, for the sets of values given in Table 5 (elastic and viscoelastic behavior of the external tissues), at the most significant coupling interfaces between the 3-D iliac (see Fig. 2b) and the 1-D network. The black line is the solution of the full 1-D network.

In Fig. 7 we compare the magnitude of the displacement field of the 3-D iliac arterial wall for the different cases. The images show that at each increase in the values of the tissues parameters, the overinflations at the branches diminish. This phenomenon is more visible in Fig. 8, where a zoomed lateral view of the top and low left bifurcations is shown. In addition, a further analysis of the flow rate and pressure wave form at the coupling interfaces (which for brevity is not presented here) shows no significant changes compared to the results in Fig. 6. In view of these results we conclude that, despite their simple formulation, Robin boundary data provide a reliable way to account for the effect of external tissues over the arterial wall. Moreover, they can be used to somehow compensate for the lack of collagen fibers in 3-D FSI models, at least in healthy arteries.

3.3.3 Solid ring boundary condition comparisons

In this section we compare the solution of geometrical multiscale models in which the boundary solid rings of the 3-D geometries are fixed, as opposed to the case where the same 3-D boundary interfaces are scaled to enforce the continuity of the vessels size with the surrounding 1-D arteries. For these comparisons we use the same geometrical multiscale models introduced in Sections 3.3.1 and 3.3.2. For the values of the elastic parameter of the external tissues, we select cases E_4^A and E_{4b}^I for the aorta and iliac, respectively, while the viscoelastic parameter is given by the relation: $c_S = k_S/10$.

In Fig. 9 and 10 several views of the magnitude difference of the two 3-D geometries displacement field are shown. In particular, we observe that a significant difference between the two cases exists only near the coupling interfaces, where the boundary conditions change. In the other parts of the wall the result is almost the same. In addition, a further analysis of the flow rate and pressure wave form at the coupling interfaces (which for brevity is not presented here) shows no significant differences between the two configurations. In view of these results we conclude that the continuity of the vessel area between 3-D and 1-D models is not essential for cardiovascular applications, unless the focus of the analysis is on the study of the dynamics and stresses of the wall near the boundary interfaces. On the contrary, it might still be relevant to avoid (or at least reduce) the generation of spurious interface wave reflections in other flow regimes, as shown in Malossi et al (2012).

3.3.4 Geometrical multiscale models comparisons

In this section we present several comparisons among different geometrical multiscale models. More precisely we compare the results of the full 1-D arterial tree described in Section 3.1, which represents an average healthy patient, with both the two dimensionally-heterogeneous models introduced in Sections 3.3.1 and 3.3.2, and a third model where the 3-D aorta and iliac patient-specific geometries are coupled together within the same 1-D network. For all the presented configurations, at the interfaces between the 3-D geometries

Table 6: Empiric external tissues coefficients at the bifurcations of the 3-D iliac (green and magenta wall regions in Fig. 2c). From the reference case $\mathrm{E}_4^{\mathrm{I}}$ (see Table 5), we define three additional configurations.

Artery	k_{S} [dyn/cm^3]				c_{S} [dyn s/cm^3]
	$\mathrm{E}_4^{\mathrm{I}}$	$\mathrm{E}_{4\mathrm{a}}^{\mathrm{I}}$	$\mathrm{E}_{4\mathrm{b}}^{\mathrm{I}}$	$\mathrm{E}_{4\mathrm{c}}^{\mathrm{I}}$	
Abdominal aorta (bifurcation)	100000	200000	300000	400000	$k_{\mathrm{S}}/10$
Left / right common iliac (bifurcations)	140000	280000	420000	560000	$k_{\mathrm{S}}/10$

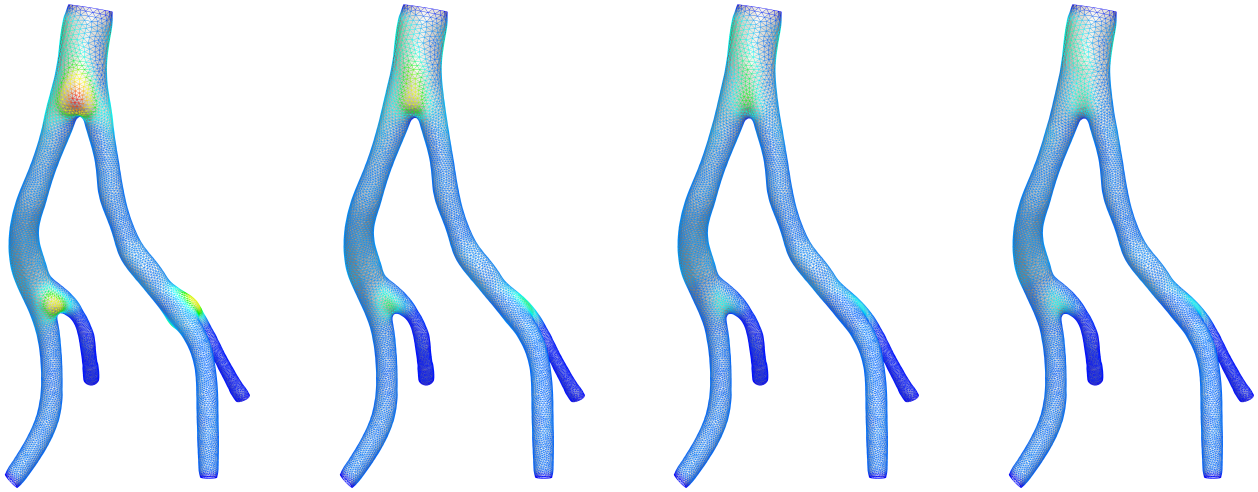

Case $\mathrm{E}_4^{\mathrm{I}}$. Case $\mathrm{E}_{4\mathrm{a}}^{\mathrm{I}}$. Case $\mathrm{E}_{4\mathrm{b}}^{\mathrm{I}}$. Case $\mathrm{E}_{4\mathrm{c}}^{\mathrm{I}}$.

Figure 7: Wall displacement magnitude comparison, at the end-systole of the third heart beat ($t = 2.0$ s), for the sets of values given in Table 6 (stiffening of the bifurcations), of the 3-D iliac (see Fig. 2c) coupled with the 1-D network (not shown). The color bar ranges from blue (0.0 cm) to red (0.5 cm).

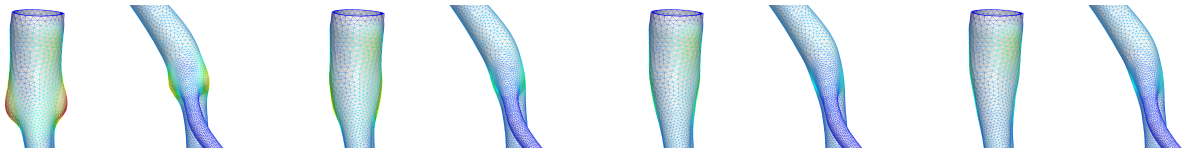

Case $\mathrm{E}_4^{\mathrm{I}}$. Case $\mathrm{E}_{4\mathrm{a}}^{\mathrm{I}}$. Case $\mathrm{E}_{4\mathrm{b}}^{\mathrm{I}}$. Case $\mathrm{E}_{4\mathrm{c}}^{\mathrm{I}}$.

Figure 8: Lateral view of the top and low left bifurcations for the four cases in Fig. 7.

and the 1-D arteries we impose the continuity of the vessel area through (6). Regarding the values of the elastic parameter of the external tissues, we select cases $\mathrm{E}_4^{\mathrm{A}}$ and $\mathrm{E}_{4\mathrm{b}}^{\mathrm{I}}$ for the aorta and iliac, respectively, while the viscoelastic parameter is given by the relation: $c_{\mathrm{S}} = k_{\mathrm{S}}/10$.

The results of the flow rate wave form comparison at all the coupling interfaces between the 1-D network and the 3-D aorta and iliac are summarized in Fig. 11 and 12, respectively. First of all, we observe that the presence of the 3-D iliac geometry does not have almost any effect on the upstream solution (apart in the thoracic aorta B interface, which is quite close to the iliac artery), while the 3-D aorta produces a visible, even if small, difference in the downstream flow (see, e.g., the external iliac interfaces). In addition, the presence of the 3-D geometries, which are not symmetric and whose branches have different left and right vessels size, changes the splitting of the flow in the network compared to the solution of the full 1-D arterial tree (see, e.g., the vertebral arteries).

Regarding the behavior of the pressure and the radial scale factor, which are shown in Fig. 13, similar comments hold. In view of these results, we conclude that 3-D patient-specific geometries might have a significant effect on the arterial flow, even in the case of healthy arteries. The presence of geometrical singularities and pathologies, such as

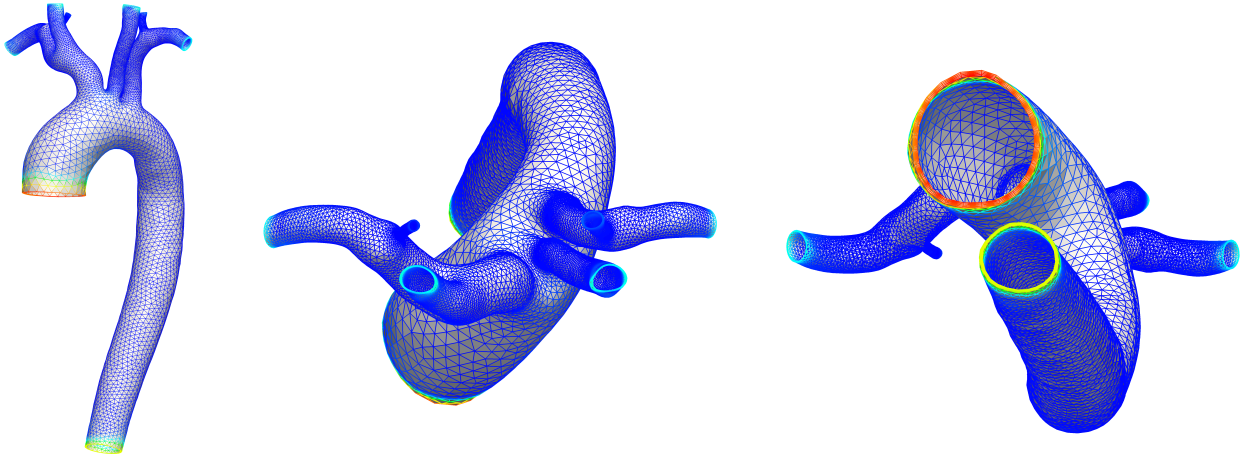

Lateral view. Top view. Bottom view.

Figure 9: 3-D aorta wall displacement magnitude difference, at the end-systole of the sixth heart beat ($t = 4.4$ s), between the scaled area and the fixed area cases. The color bar ranges from blue (0.0 cm) to red (0.2 cm).

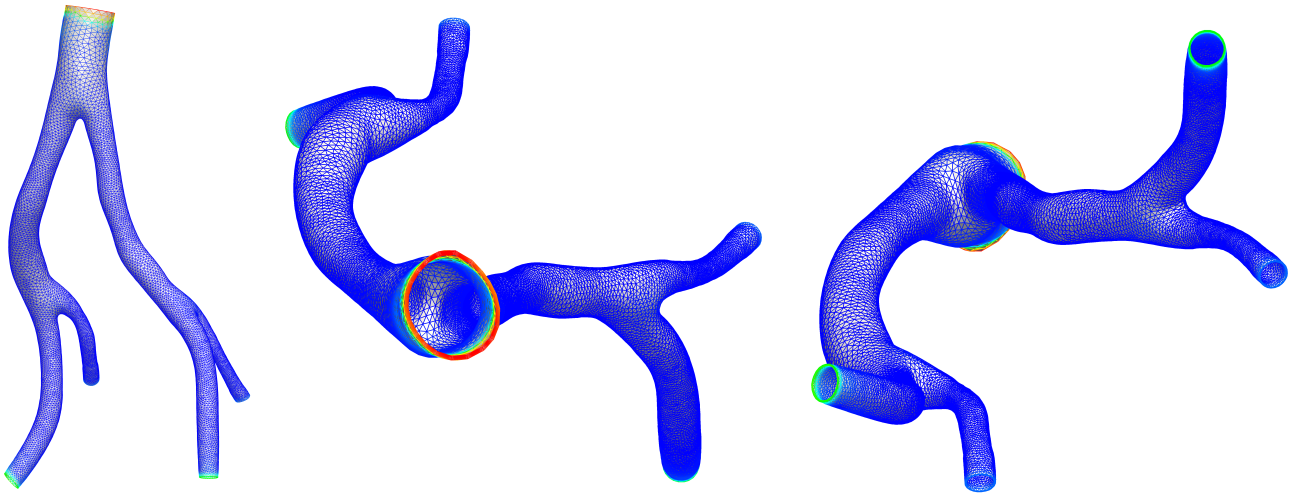

Lateral view. Top view. Bottom view.

Figure 10: 3-D iliac wall displacement magnitude difference, at the end-systole of the sixth heart beat ($t = 4.4$ s), between the scaled area and the fixed area cases. The color bar ranges from blue (0.0 cm) to red (0.1 cm).

aneurysms and stenoses, would probably increase this effect and it will be subject of future works.

3.4 Stand-alone 3-D FSI modeling

In this section we set up a comparison between the results of the geometrical multiscale models presented in Sections 3.3.1 and 3.3.2, and their stand-alone 3-D FSI simulations counterparts. More precisely, the stand-alone 3-D problems are set up by considering the same 3-D geometries and data used in the two reference geometrical multiscale models (cases E_4^A and E_{4b}^I, respectively, with $c_S = k_S/10$). However, at the boundary interfaces, instead of imposing the set of conservation equations with the surrounding models, as described in Section 2.3, we prescribe either flow rate or stress time profiles, taken from a precomputed solution of a full 1-D arterial tree. Following the same approach, we also impose the radial scale factor time profile on the solid ring boundary interfaces, such that they are not fixed.

The flow rate and pressure wave form comparisons, at the most significant coupling interfaces between the 3-D aorta and the 1-D network, are summarized in Fig. 14. The results

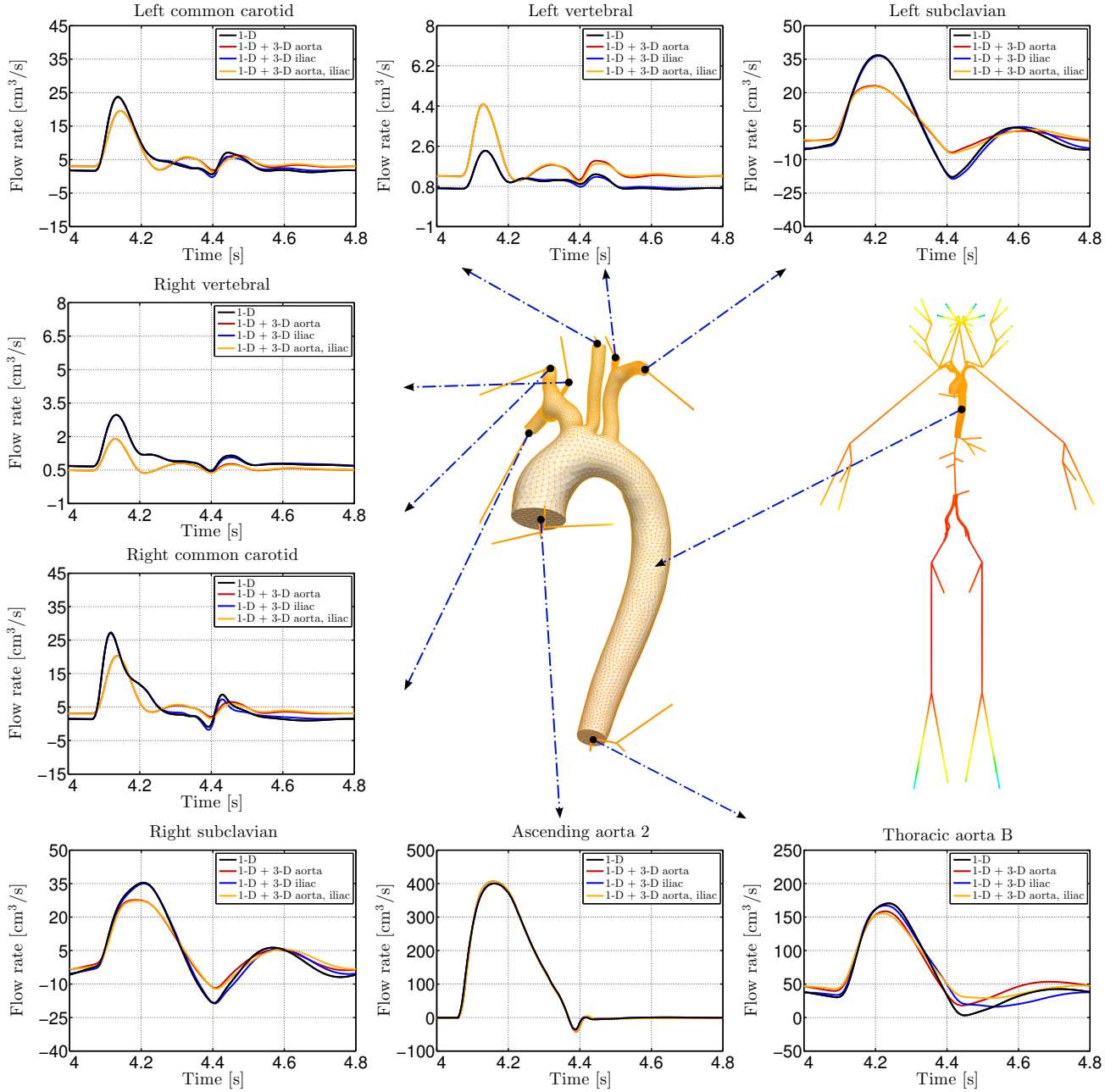

Figure 11: Flow rate comparison, at the sixth heart beat, for different configurations of the global arterial network, at the eight interfaces of the 3-D aorta. The color of the 3-D images represents the pressure field at the end-systole of the sixth heart beat ($t = 4.4$ s), where the color bar ranges from blue (80000 dyn/cm^2) to red (165000 dyn/cm^2). Positioning of 1-D network elements is purely visual.

show significant differences between the reference configuration, i.e., the geometrical multiscale model, and the solution computed by solving the stand-alone 3-D aorta model. Let us consider for instance the flow rate wave form. The red lines coincide with the precomputed (and imposed) solution of the full 1-D arterial tree, which is different from the one of the geometrical multiscale model, as already discussed in Section 3.3.4. On the contrary, the blue lines are computed by imposing a stress boundary data. However, even in this case, the resulting flow rate is significantly different from the reference one. In particular, the flow rate prediction in the left common carotid and vertebral arteries are clearly incorrect. Regarding the pressure wave form, where the precomputed solution of the full 1-D arterial network coincides with the blue lines, a visible vertical gap between the reference solution and the stand-alone cases is always present. In

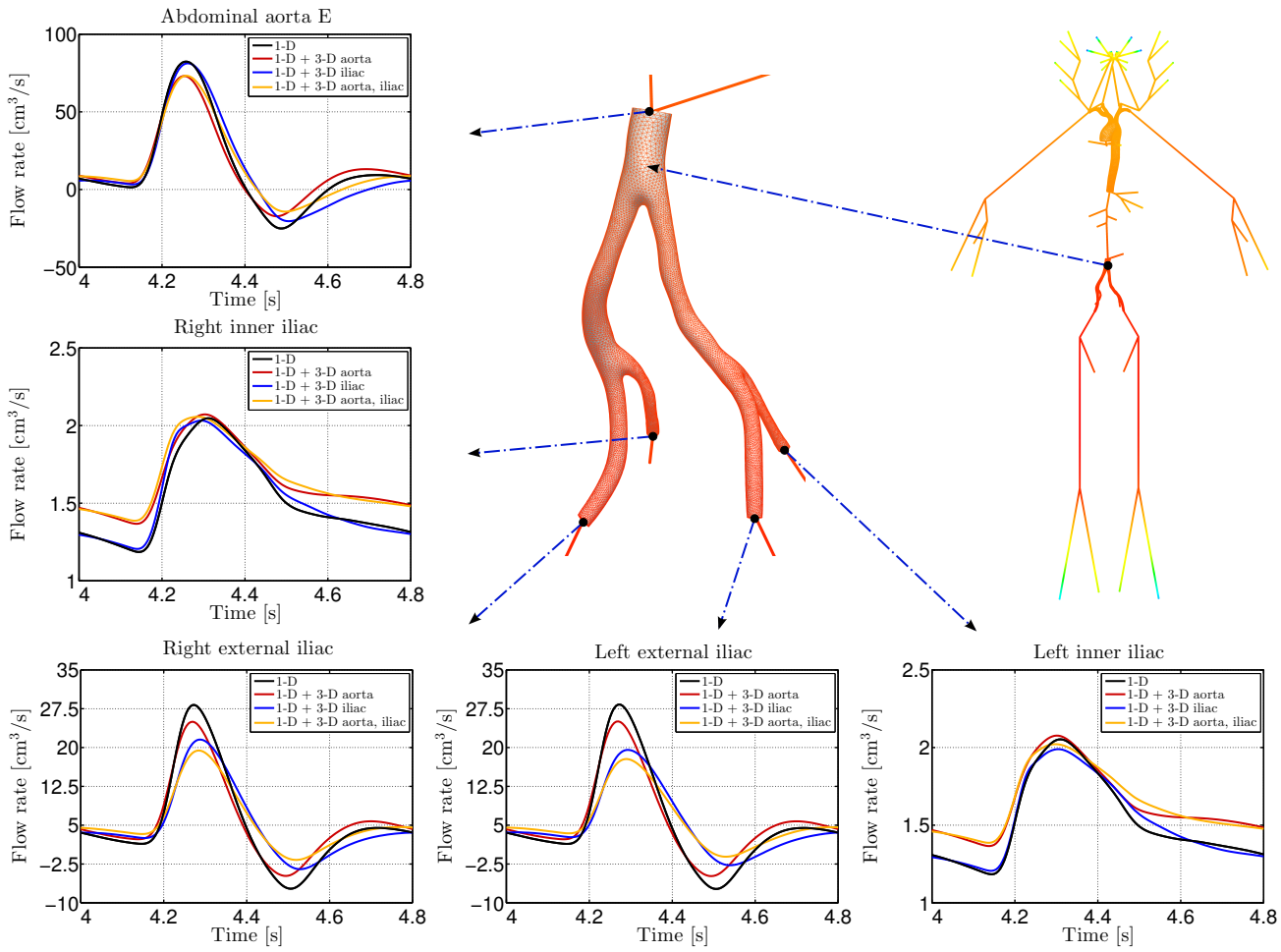

Figure 12: Flow rate comparison, at the sixth heart beat, for different configurations of the global arterial network, at the five interfaces of the 3-D iliac. The color of the 3-D images represents the pressure field at the end-systole of the sixth heart beat ($t = 4.4$ s), where the color bar ranges from blue (80000 dyn/cm^2) to red (165000 dyn/cm^2). Positioning of 1-D network elements is purely visual.

particular, the average pressure level is overestimated when the flow rate is imposed, and underestimated when the stress is prescribed. As a consequence of the different flow rate and pressure wave form, also the displacement field changes, as shown in Fig. 15. The differences in respect to the reference case are more evident when imposing the flow rate, where we also observe a non-physiological overinflation of the left common carotid artery, even if we use the same values for the tissues parameters in both simulations.

Regarding the stand-alone 3-D iliac model, similar considerations hold, as shown in Fig. 16, and 17. Among other things, we highlight the totally incorrect flow rate prediction in the left inner iliac artery when imposing a stress boundary data.

The results of these comparisons prove the importance of the geometrical multiscale approach in the modeling of cardiovascular flows. The different behavior of the stand-alone 3-D FSI simulations in respect to the geometrical multiscale model reference cases is mainly due to the lack of dynamic interplay between the dimensionally-heterogeneous models. Indeed, on the one hand, the set of conservation equations described in Section 2.3 provides a reliable and automatic way to determine the boundary data of each coupled model. In addition, on the other hand, they also provide bilateral information on both flow rate and pressure, independently from the imposed boundary condition type.

4 Conclusions

In this work, we presented several numerical comparisons of geometrical multiscale models. A brief description of the main ingredients of the geometrical multiscale approach has been recalled from previous works, together with the parti-

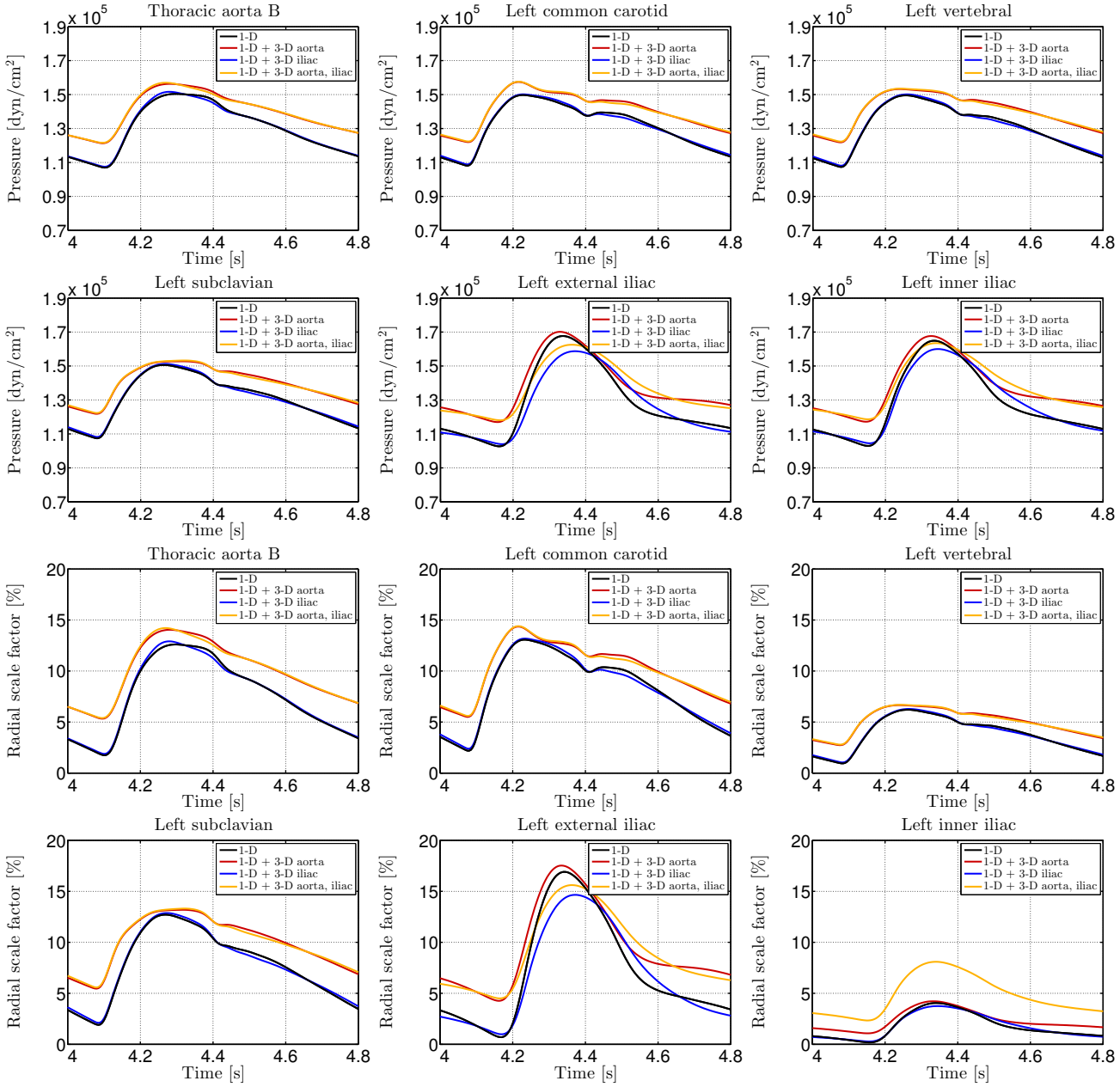

Figure 13: Pressure and radial scale factor comparisons, at the sixth heart beat, for different configurations of the global arterial network, at the most significant coupling interfaces of the 3-D aorta and iliac (see Fig. 11 and 12).

tioned solution strategy used to set up the global network of dimensionally-heterogeneous models.

The purposes of this work were manifold. A first goal was to provide a systematic approach to set up geometrical multiscale models, and to give more insight on the calibration of the most critical parameters needed by the numerical simulations. In this regard we first provided a short description of the procedure required to plug one or more 3-D patient-specific geometries in a 1-D arterial tree network, whose parameters were calibrated to represent an average healthy patient. Then we set up several comparisons to study the sensitivity of the main quantities of interest (flow rate, pressure, and solid wall displacement) in respect to the elastic and viscoelastic external tissues parameters. These quantities, which appear in the Robin boundary condition on the solid wall of the 3-D FSI models, are empiric coefficients whose evaluation is rather difficult. The results of our analysis show that:

1. purely elastic Robin boundary conditions are not adequate to represent the physical behavior of the arterial wall;

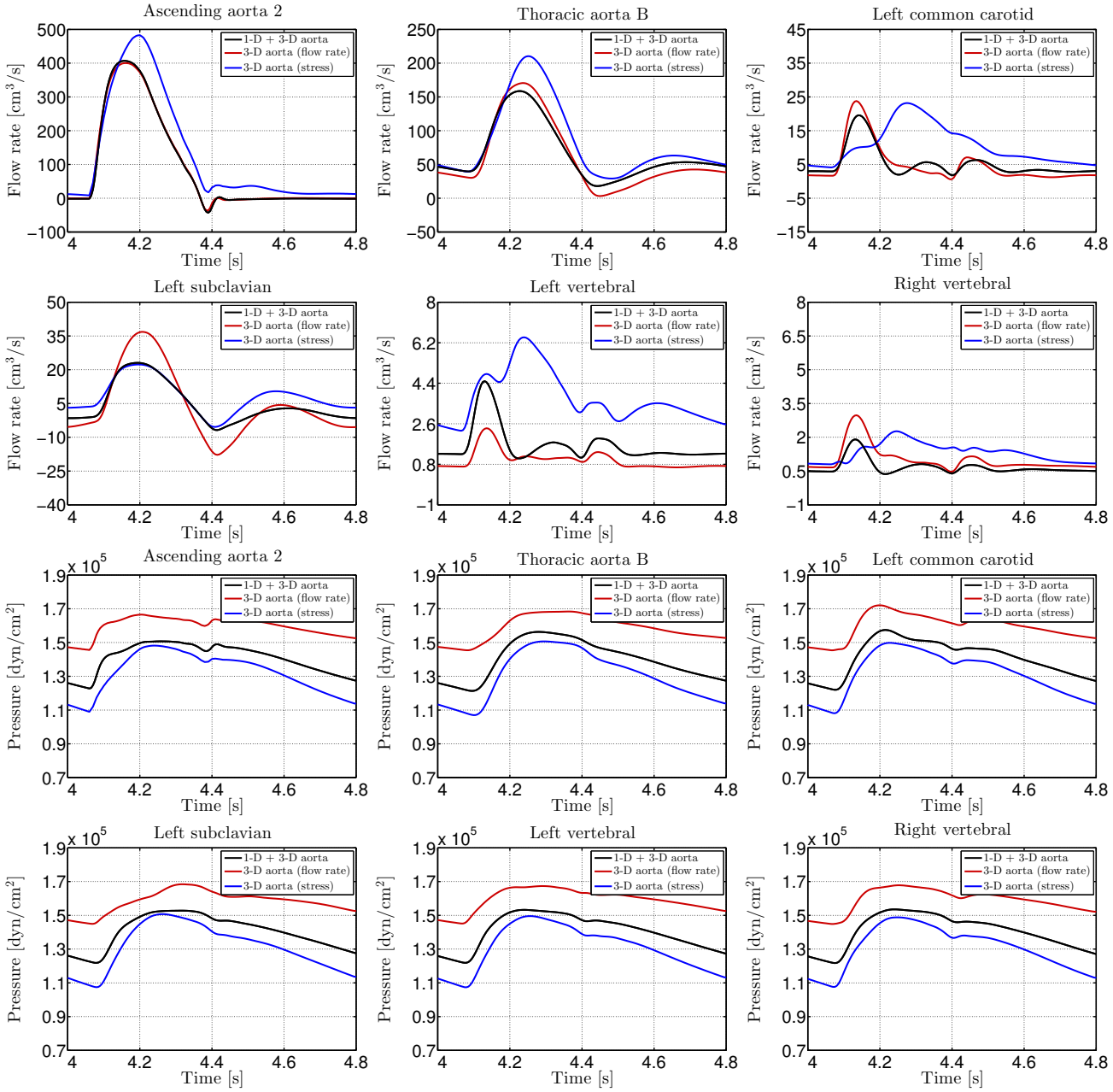

Figure 14: Flow rate and pressure comparisons, at the sixth heart beat, between the solution of the geometrical multiscale problem and the one of the stand-alone 3-D aorta with flow rate or stress boundary data from the full 1-D network, at the most significant coupling interfaces of the 3-D aorta.

2. a simple empiric relation can be used to determine the value of the viscoelastic parameter as a function of the elastic one;
3. above a certain threshold, the sensitivity of the flow rate and pressure wave form to a variation of the external tissues parameters is very small;
4. Robin boundary data can also be used to somehow compensate for the lack of collagen fibers in 3-D FSI models, at least in healthy arteries.

Therefore, we showed that it is possible to estimate, in a systematic way, an admissible range of values for these parameters, such that they lead to reliable physiological results.

Another goal of this work was to prove the importance of the geometrical multiscale approach in the modeling of cardiovascular flows. To do this we compared the results given by geometrical multiscale models with both the solution of a full 1-D arterial tree, and the one of stand-alone 3-D problems, where the 3-D patient-specific geometries were fed

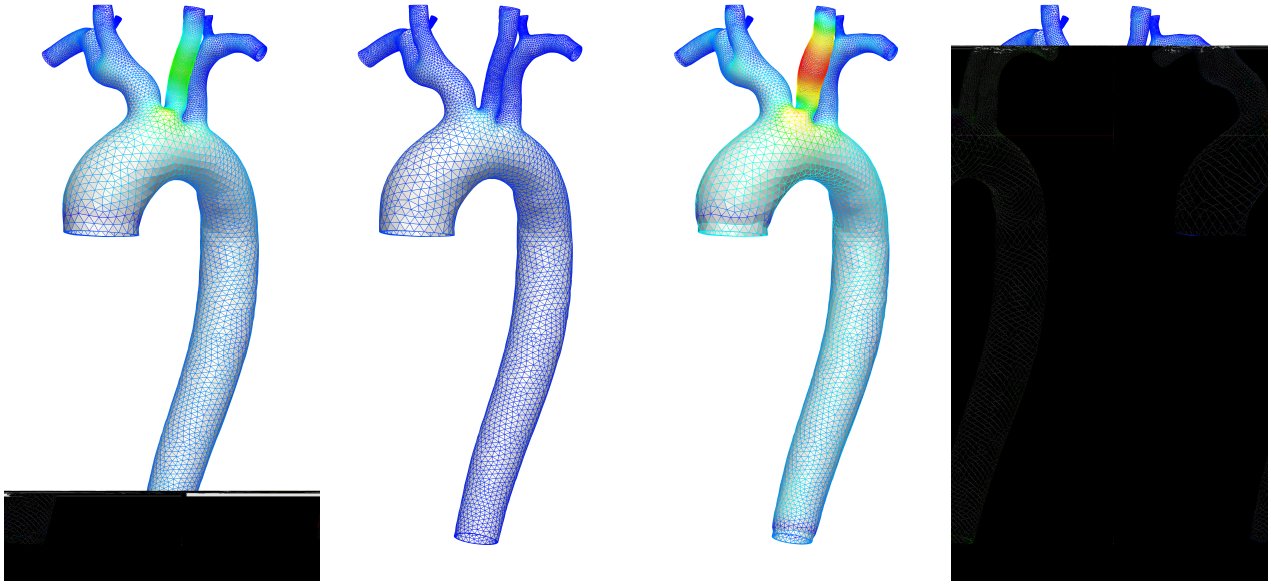

Flow rate imposed ($t = 4.4$ s). Stress imposed ($t = 4.4$ s). Flow rate imposed ($t = 4.8$ s). Stress imposed ($t = 4.8$ s).

Figure 15: 3-D aorta wall displacement magnitude difference, at the end-systole and end-diastole of the sixth heart beat, between the solution of the geometrical multiscale problem and the one of the stand-alone 3-D aorta with flow rate or stress boundary data from the full 1-D network. The color bar ranges from blue (0.0 cm) to red (0.5 cm).

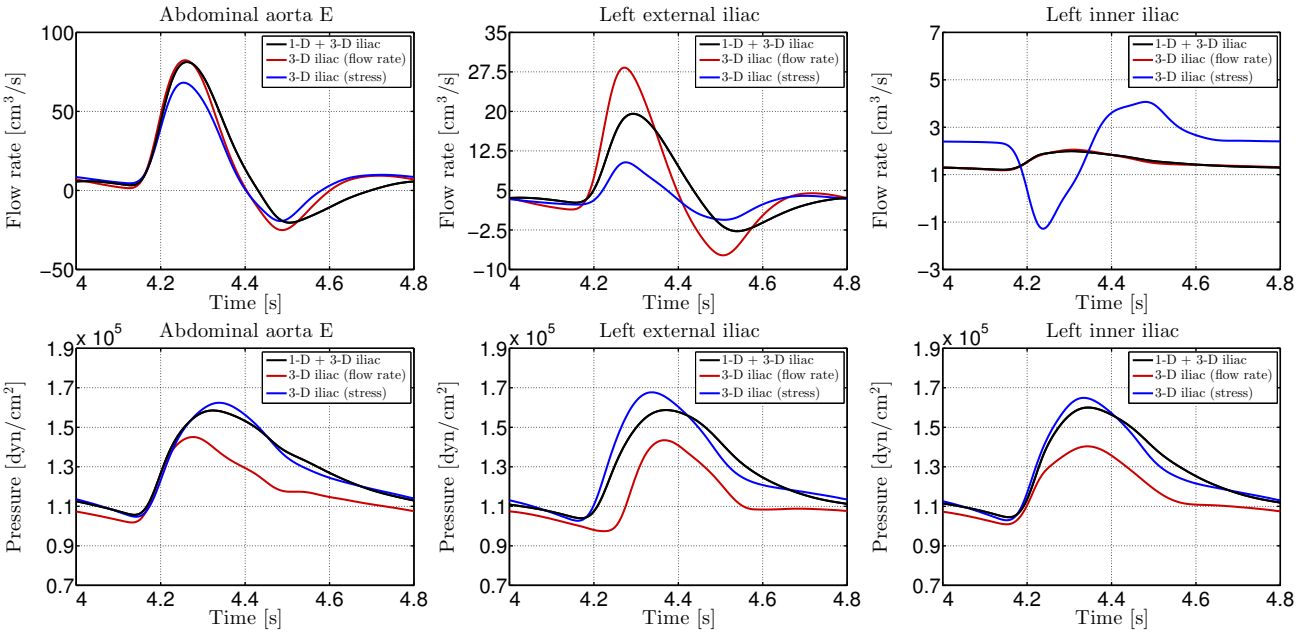

Figure 16: Flow rate and pressure comparisons, at the sixth heart beat, between the solution of the geometrical multiscale problem and the one of the stand-alone 3-D iliac with flow rate or stress boundary data from the full 1-D network, at the most significant coupling interfaces of the 3-D iliac.

with boundary data taken from a precomputed solution of the same full 1-D network. Main results of this analysis are:

1. 3-D patient-specific geometries might produce significant changes in the 1-D arterial flow, even in the case of healthy arteries;

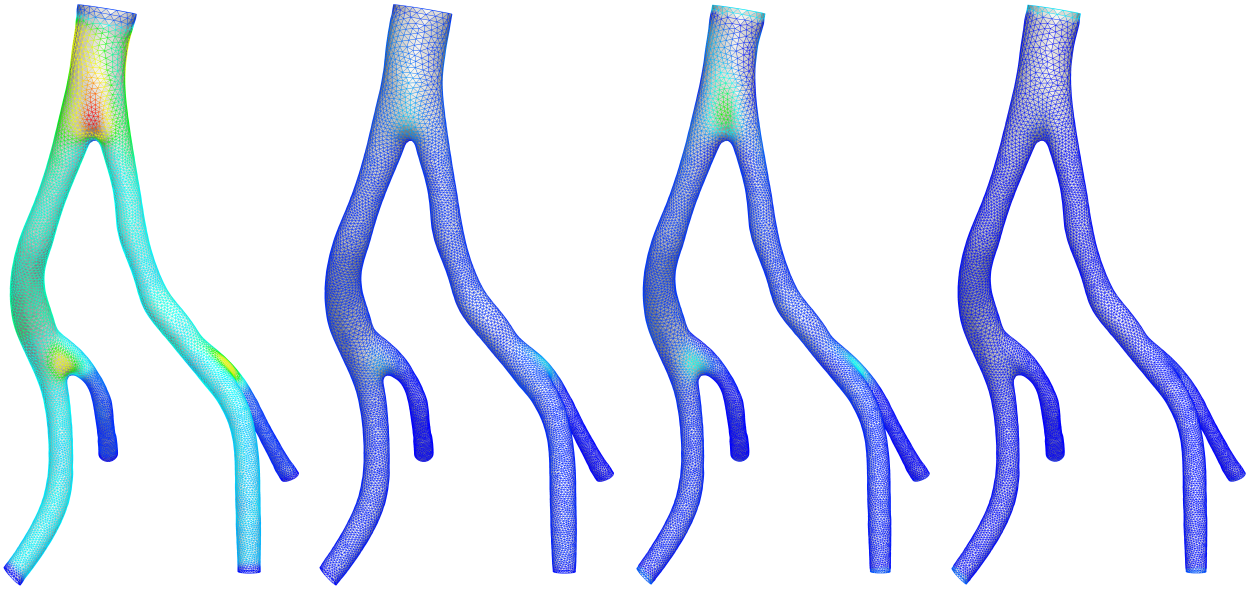

Flow rate imposed ($t = 4.4$ s). Stress imposed ($t = 4.4$ s). Flow rate imposed ($t = 4.8$ s). Stress imposed ($t = 4.8$ s).

Figure 17: 3-D iliac wall displacement magnitude difference, at the end-systole and end-diastole of the sixth heart beat, between the solution of the geometrical multiscale problem and the one of the stand-alone 3-D iliac with flow rate or stress boundary data from the full 1-D network. The color bar ranges from blue (0.0 cm) to red (0.5 cm).

2. stand-alone 3-D FSI simulations are not able to capture the correct flow rate and pressure wave form, since they lack the dynamic interplay among the dimensionally-heterogeneous models;
3. the continuity of the vessel area between 3-D and 1-D FSI models is not essential for cardiovascular applications, unless the focus of the analysis is on the study of the dynamics and stresses of the wall near the boundary interfaces.

In view of these results we proved that, despite their increased complexity and computational cost, geometrical multiscale models provide more accurate results compared to purely 1-D arterial networks or simpler stand-alone 3-D FSI simulations. Indeed, they give the possibility to specifically study regions of interest by the mean of 3-D FSI models, evaluating local hemodynamics parameters (e.g., wall shear stress, turbulent flow, regions of recirculation) without neglecting the interaction with the global circulation. In future works, the present methodology (eventually extended) will be used to set up numerical simulations in the context of patient-specific medicine, i.e., for the diagnosis, treatment, and follow-up of specific diseases and pathologies.

Acknowledgements A. C. I. Malossi acknowledges the Swiss Platform for High-Performance and High-Productivity Computing (HP2C). J. Bonnemain acknowledges the Swiss National Fund (SNF) grant 323630-133898. We also acknowledge the European Research Council Advanced Grant "Mathcard, Mathematical Modelling and Simulation of the Cardiovascular System", Project ERC-2008-AdG 227058. Last but not least, we acknowledge Pablo Blanco (LNCC) and Simone Deparis (CMCS, EPFL) for their precious support, as well as Phylippe Reymond (LHTC, EPFL) for the 3-D geometries of aorta and iliac arteries. All the numerical results presented in this paper have been computed using the `LifeV` library (`www.lifev.org`).

References

Alastruey J, Parker KH, Peiró J, Byrd SM, Sherwin SJ (2007) Modelling the circle of Willis to assess the effects of anatomical variations and occlusions on cerebral flows. J Biomech 40(8):1794–1805

Blanco PJ, Feijóo RA, Urquiza SA (2007) A unified variational approach for coupling 3D–1D models and its blood flow applications. Comp Meth Appl Mech Engrg 196(41–44):4391–4410

Blanco PJ, Leiva JS, Feijóo RA, Buscaglia GC (2011) Black-box decomposition approach for computational hemodynamics: One-dimensional models. Comp Meth Appl Mech Engrg 200(13–16):1389–1405

Bonnemain J, Faggiano E, Quarteroni A, Deparis S (2012) A patient-specific framework for the analysis of the haemodynamics in patients with ventricular assist device, submitted

Burman E, Fernández MA, Hansbo P (2006) Continuous interior penalty finite element method for Oseen's equations. SIAM J Numer Anal 44(3):1248–1274

Crosetto P (2011) Fluid-structure interaction problems in hemodynamics: Parallel solvers, preconditioners, and applications. PhD thesis, EPFL

Crosetto P, Deparis S, Fourestey G, Quarteroni A (2011a) Parallel algorithms for fluid-structure interaction problems in haemodynamics. SIAM J Sci Comput 33(4):1598–1622

Crosetto P, Reymond P, Deparis S, Kontaxakis D, Stergiopulos N, Quarteroni A (2011b) Fluid-structure interaction simulation of aortic blood flow. Comput Fluids 43(1):46–57

Crosetto P, Deparis S, Formaggia L, Mengaldo G, Nobile F, Tricerri P (2012) A comparative study of different nonlinear hyperelastic isotropic arterial wall models in patient-specific vascular flow simulations in the aortic arch, submitted

Formaggia L, Nobile F, Quarteroni A, Veneziani A (1999) Multiscale modelling of the circulatory system: a preliminary analysis. Comput Visual Sci 2(2–3):75–83

Formaggia L, Lamponi D, Quarteroni A (2003) One-dimensional models for blood flow in arteries. J Eng Math 47(3–4):251–276

Formaggia L, Moura A, Nobile F (2007) On the stability of the coupling of 3D and 1D fluid-structure interaction models for blood flow simulations. ESAIM: Mathematical Modelling and Numerical Analysis 41(4):743–769

Formaggia L, Quarteroni A, Veneziani A (2009) Cardiovascular Mathematics, Modeling, Simulation and Applications, vol 1. Springer-Verlag, Milan

Fung YC (1993) Biomechanics: Mechanical Properties of Living Tissues, 2nd edn. Springer-Verlag, New York

Holzapfel GA, Ogden RW (2006) Mechanics of Biological Tissue. Springer-Verlag, Berlin Heidelberg

Holzapfel GA, Gasser TC, Ogden RW (2000) A new constitutive framework for arterial wall mechanics and a comparative study of material models. J Elasticity 61(1–3):1–48

Kanyanta V, Ivankovic A, Karac A (2009) Validation of a fluid-structure interaction numerical model for predicting flow transients in arteries. J Biomech 42(11):1705–1712

Langewouters GJ (1982) Visco-elasticity of the human aorta in vitro in relation to pressure and age. PhD thesis, Free University, Amsterdam

Liu Y, Dang C, Garcia M, Gregersen H, Kassab GS (2007) Surrounding tissues affect the passive mechanics of the vessel wall: theory and experiment. Am J Physiol Heart Circ Physiol 293(6):H3290–H3300

Malossi ACI, Blanco PJ, Deparis S (2011a) A two-level time step technique for the partitioned solution of one-dimensional arterial networks, submitted

Malossi ACI, Blanco PJ, Deparis S, Quarteroni A (2011b) Algorithms for the partitioned solution of weakly coupled fluid models for cardiovascular flows. Int J Num Meth Biomed Engng 27(12):2035–2057

Malossi ACI, Blanco PJ, Crosetto P, Deparis S, Quarteroni A (2012) Implicit coupling of one-dimensional and three-dimensional blood flow models with compliant vessels, submitted

Moireau P, Xiao N, Astorino M, Figueroa CA, Chapelle D, Taylor CA, Gerbeau JF (2012) External tissue support and fluid-structure simulation in blood flows. Biomech Model Mechanobiol 11(1–2):1–18

Papadakis G (2009) Coupling 3D and 1D fluid-structure-interaction models for wave propagation in flexible vessels using a finite volume pressure-correction scheme. Commun Numer Meth Engng 25(5):533–551

Reymond P, Merenda F, Perren F, Rüfenacht D, Stergiopulos N (2009) Validation of a one-dimensional model of the systemic arterial tree. Am J Physiol Heart Circ Physiol 297(1):H208–H222

Reymond P, Bohraus Y, Perren F, Lazeyras F, Stergiopulos N (2011) Validation of a patient-specific one-dimensional model of the systemic arterial tree. Am J Physiol Heart Circ Physiol 301(3):H1173–H1182

Shi Y, Lawford P, Hose R (2011) Review of Zero-D and 1-D models of blood flow in the cardiovascular system. BioMedical Engineering OnLine 10(33):1–38

Vignon-Clementel IE, Figueroa CA, Jansen KE, Taylor CA (2006) Outflow boundary conditions for three–dimensional finite element modeling of blood flow and pressure in arteries. Comp Meth Appl Mech Engrg 195(29–32):3776–3796

Recent publications :

MATHEMATICS INSTITUTE OF COMPUTATIONAL SCIENCE AND ENGINEERING
Section of Mathematics
Ecole Polytechnique Fédérale
CH-1015 Lausanne

03.2012 T. LASSILA, A. MANZONI, A. QUARTERONI, G. ROZZA:
Boundary control and shape optimization for the robust design of bypass anastomoses under uncertainty

04.2012 D. KRESSNER, C. TOBLER:
htucker – A Matlab toolbox for tensors in hierarchical Tucker format

05.2012 A. ABDULLE, G. VILLMART, KONSTANTINOS C. ZYGALAKIS:
Second weak order explicit stabilized methods for stiff stochastic differential equations

06.2012 A. CABOUSSAT, S. BOYAVAL, A. MASSEREY:
Three-dimensional simulation of dam break flows

07.2012 J BONNEMAIN, S. DEPARIS, A. QUARTERONI:
Connecting ventricular assist devices to the aorta: a numerical model

08.2012 J BONNEMAIN, ELENA FAGGIANO, A. QUARTERONI, S. DEPARIS:
A framework for the analysis of the haemodynamics in patient with ventricular assist device

09.2012 T. LASSILA, A. MANZONI, G. ROZZA:
Reduction strategies for shape dependent inverse problems in haemodynamics

10.2012 C. MALOSSI, P. BLANCO, P. CROSETTO, S. DEPARIS, A. QUARTERONI:
Implicit coupling of one-dimensional and three-dimensional blood flow models with compliant vessels

11.2012 S. FLOTRON J. RAPPAZ:
Conservation schemes for convection-diffusion equations with Robin's boundary conditions

12.2012 A. UMSCHMAJEW, B. VANDEREYCKEN:
The geometry of algorithms using hierarchical tensors

13.2012 D. KRESSNER, B. VANDEREYCKEN:
Subspace methods for computing the pseudospectral abscissa and the stability radius

14.2012 B. JEURIS, R. VANDEBRIL, B. VANDEREYCKEN:
A survey and comparison of contemporary algorithms for computing the matrix geometric mean

15.2012 A. MANZONI, A. QUARTERONI, G. ROZZA:
Computational reduction for parametrized PDEs: strategies and applications

16.2012 A.C.I. MALOSSI, J. BONNEMAIN:
Numerical comparison and calibration of geometrical multiscale models for the simulation of arterial flows